國 立 交 通 大 學

電 機 與 控 制 工 程 學 系

碩 士 論 文

應用於 VDSL 系統之最佳化功率分配

Optimal Power Allocation for VDSL System

研 究 生：張 孟 良

指 導 教 授：林 源 倍 博士

中華民國九十三年六月

應用於 VDSL 系統之最佳化功率分配

Optimal Power Allocation for VDSL System

研 究 生：張孟良　　Student：Meng-Liang Chang

指導教授：林源倍博士　Advisor：Dr. Yuan-Pei Lin

國 立 交 通 大 學

電 機 與 控 制 工 程 學 系

A Thesis

Submitted to Institute of Electrical and Control Engineering

College of Electrical Engineering and Information Science

National Chiao Tung University

In Partial Fulfillment of the Requirements

For the Degree of Master

In

Electrical and Control Engineering

June 2004

Hsinchu, Taiwan, Republic of China

中華民國九十三年六月

應用於 VDSL 系統之最佳化功率分配

學生：張孟良　　指導教授：林源倍博士

國立交通大學電機與控制工程學系（研究所）碩士班

摘　　要

近來非常高速數位迴路(VDSL)系統應用於高速資料傳輸的發展上引起廣泛的興趣。VDSL 系統使用具有非平的功率頻譜遮罩的多頻帶頻率分配。在這種情況下，傳統的 water-filling 功率分配可能不是最好的選擇。在本論文中，我們考慮一種最佳化的功率分配應用於具有非平的功率頻譜遮罩的離散多調(DMT)系統。我們可以看到，使用最佳化功率分配將比一般使用的功率分配達到較高的傳輸速率。

Optimal Power Allocation for VDSL System

Student : Meng-Liang Chang Advisor : Yuan-Pei Lin

Department of Electrical and Control Engineering
National Chiao Tung University

Abstract

Recently there has been great interest in the development of VDSL (very-high-bit-rate digital subscriber line) system for high speed data transmission systems. The VDSL system has multiband frequency plan with a non-flat power spectrum mask. In this case, the conventional water-filling power allocation may not be the best thing to do. In this thesis, we consider optimal power allocation for DMT (discrete multitone) systems with a non-flat power spectrum density mask. We will see that, the optimal power allocation will achieve higher data rate than the commonly used power allocation.

誌謝

本論文得以順利完成，有賴許多師長的協助。首先要感謝恩師林源倍老師二年來的指導與栽培，在我遇到困境時，適時的給予幫助與解惑。老師待人處事及嚴謹的治學態度，亦是我最好的身教。同時也感謝口試委員林清安及鄭木火教授在百忙之中抽空給予指導與建議，使本文得以更加完備。還有立人、昶誠和重慶學長，以及同門諸友的幫助與鼓勵，都是這些日子以來不可或缺的支持。也因為你們，使我的求學生涯更加多采。在此更要感謝我的父母以及家人的支持與協助，讓我沒有後顧之憂，得以順利完成學業。以及許許多多曾經幫助與支持我的朋友們，感謝大家一路上的提攜。在此，願大家在人生路上都能幸福、快樂、順利。

張孟良　謹誌

民國九十三年

Contents

List of Figures

List of Tables

Chapter 1

Introduction

The application of Multicarrier Modulation (MCM) scheme has received a great interest these years due to the enormous advances in very-large-scale integrated (VLSI) circuits and digital signal processing (DSP). Especially, DFT based (Discrete Fourier Transform) transceiver can be implemented in wireline and wireless transmissions. In wireline transmission, usually is called DMT (Discrete Multitone), it has wide applications in DSL (Digital Subscriber Lines), such as ADSL (Asymmetric DSL) and HDSL (High-speed DSL). In particular, the ADSL aims at providing high bandwidth within the 18 kilo feet CSA (carrier serving area). It promises a downstream data rate from 1.5 Mega bits/sec to 8 Meta bits/sec and a upstream data rate around 1/10 the downstream data rate. These DSL transmission technologies utilize the existing telephone line network infrastructure, hence can provide high speed transmission at very low cost. Recently, the new DSL technology, VDSL (Very-high-bit-rate DSL), has been proposed for the more high-speed transmission. Up to 52 Mega bits/sec downstream for asymmetric applications and 26 Mega bits/sec two-way for symmetric applications can be achieved by VDSL. Ultimately, VDSL would support high-definition television (HDTV) and high-performance computing applications.

In DMT scheme, the channel is partitioned into subchannels, each with a different frequency band. The input bit stream is parsed and coded as modulation symbols, e.g., PAM or QAM (pulse or quadrature amplitude modulation), and these symbols are inputs of the transmitting filters. Modulation symbols of

different suhchannels can carry different number of bits depending on the SNR (signal-to-noise ratio) in the subchannels. The DMT systems that have been studied so far are mostly DFT based as shown in Fig. 1.1.

The DFT based DMT transceiver has found applications in a wide range of transmission channels. The transmitter and receiver perform respectively M-point IDFT and DFT computation, where M is the number of tones or number of subchannels. At the transmitter side, each block is padded with a cyclic prefix of length L. If L is no smaller than the order of the channel, which is usually assumed to be an FIR filter after proper equalization, inter-block ISI can be removed by discarding the prefix at the receiver. The outputs of the DFT matrix are multiplied by one-tap frequency domain equalizers equal to the DFT of the channel impulse response. In this case, the receiver outputs are the same as the transmitter inputs in the absence of noise. As a result, the DFT based DMT system can be viewed as a set of M parallel additive-Gaussian subchannels with different noise variance for each subchannel as shown in Fig. 1.2, where x_k is the input, n_k is the equivalent noise with variance N_k and s_k is the output for the kth subchannel. Given the noise variances, probability of error and total transmission power budget, the power can be allocated optimally to achieve maximum transmission rate. The solution is known as water-filling power loading. In such a problem setup, only the total transmission power is constrained but there is no constraint on the maximum power that can be allocated to each tone (subchannel).

In this thesis, we consider the power loading problem with constraints on the maximum power and minimum power that can be allocated to each tone. The motivation of such a constrained power loading is two-fold. In some applications, e.g., VDSL system, the power spectral density mask of the transmitted signal is non-flat. This in effect imposes restrictions on the power allocated to individual tones, different maximum power constraints for different tones . On the other hand, conventional water-filling solution does not constrain the minimum non-zero power allocated to tones. Many tones will be allocated power that is not sufficient to transmit any bit, given the desired probability of error. In this case,

the power allocated to these tones will go wasted. In this thesis, we will derive the optimal solution of constrained power loading for bit rate maximization. Simulation examples will be given to demonstrate that a higher transmission rate can be achieved for VDSL sytesm.

1.1 Outline

In Chapter 2, we will study the DMT system model including loop characteristics and impairments. In Chapter 3, DFT based VDSL system will be investigated. And a filterbank representation that gives a simple expression of the PSD of the transmitting signal is introduced. In Chapter 4, we will introduce the optimal power allocation to maximize the data rate. In Chapter 5, some experiments will be shown and comparison of these two power allocation methods will be given. And a conclusion will be drawn in Chapter 6.

1.2 Notations

1. **Boldfaced** lowercases and **Boldfaced** uppercases denote vectors or matrices, respectively.

2. L denote the order of desired equalized channel impulse response.

3. Channel is modeled by a rational transfer function

$$H(z) = z^{-d} \frac{\sum_{k=0}^{L} p_k z^{-k}}{B(z)}$$

4. The notation W_M^k is used to represent the value given by

$$W_M^k = \frac{1}{\sqrt{M}} e^{-j\frac{2\pi}{M}k}$$

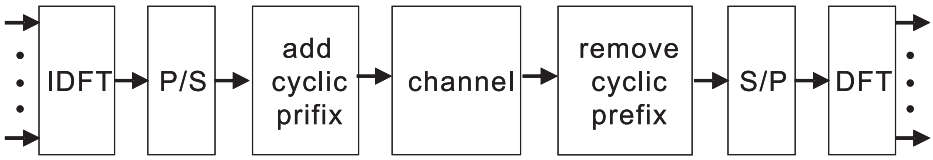

Figure 1.1: Block diagram of DFT based DMT system

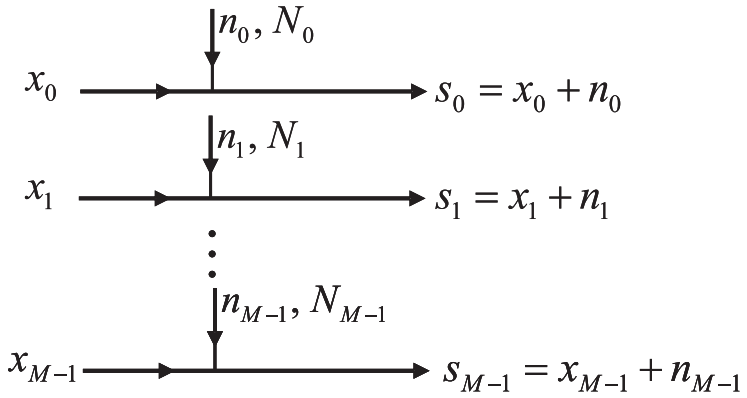

Figure 1.2: Equivalent parallel additive-Gaussian subchannels for DFT based DMT system

Chapter 2

DMT System Model

In this chapter, loop characteristics and their impairments will be introduced and the system model will be given.

2.1 Loop Characteristics

Twisted pairs are often characterized by their gauge using American Wire Gauge (AWG) designations and the gauge is indicative of the diameter of the copper wires making up the twisted pair with the smaller gauge number corresponding to the larger diameter. Fig. 2.1 shows the test loops for VDSL system and Table 2.1 gives the parametric length given in [5]. In our simulations, the detail characteristic of test loops, e.x., aerial or underground cable, isn't took into account. The data transmission system over VDSL loops are susceptible to various types of impairment. Possible impairments include:

1. Inter-symbol Interference (ISI): This is caused by non-ideal channel response and can be cancelled by well designed transceivers.

2. Crosstalk Noise: Such noise results from coupling of adjacent loops within the same cable bundle and can be modeled as two terms, the near-end crosstalk (NEXT) and far-end crosstalk (FEXT). The two main deployment scenarios,Fiber-To-The-Exchange (FTTEx) and Fiber-To-The-Cabinet (FTTCab), are considered for noise model definition. Each scenario results n a length-dependent PSD of noise, reflection the distance

between the exchange and the cabinet (L1) and also distances L2 and L3 as described in Fig. 2.2. In the FFTCab scenario, the noise should be attenuated by the value which reflects the attenuation of the corresponding signals while propagating from the exchange to the cabinet. For modeling purposes, length L1 is ste to 3281 ft, length L2 is ste equal to the length of the applicable test loop, length L3 is set to 0 kft. In the VDSL application, the NEXT and FEXT can be modeled as transfer functions given by

$$|H_{next}(f,L)|^2 = K_{nest}(1/49)^{0.6} f^{1.5}[1 - |H(f,L)|^4] \tag{2.1}$$

and

$$|H_{fext}(f,L)|^2 = |H(f,L)|^2 K_{fext}(1/49)^{0.6} L f^2, \tag{2.2}$$

where $|H(f,L)|$ is the magnitude of loop insertion gain transfer function, K_{next} and K_{fext} are crosstalk coupling coefficients, L is loop length in feet, and f is frequency in Hertz. For category-5 twisted pair, the coefficient $K_{next} = 8.818 \times 10^{-14}$ changes to $K_{next-cat5} = 3.30 \times 10^{-16}$ and the coefficient $K_{fext} = 7.999 \times 10^{-20}$ changes to $K_{fext-cat5} = 2.44 \times 10^{-22}$.

3. Additive White Gaussian Noise (AWGN): Electric noise such as quantization noise in A/D and D/A converters and thermal noise in the analog portion of the transceiver will be modeled as AWGN. In our discussion, the AWGN level is -140 dBm/Hz.

4. Other Noise: Impulse noise which caused by switching transients, lighting and other electrical machinery and Radio frequency interference (RFI) produced by the broadcast, e.g., AM/FM, or other amateur radio noise are ignored in our discussion.

Detail specification of the test loops and impairments can be found in [5] and [6].

2.2 DMT System Model

Fig. 2.3(a) shows the block diagram form transmitter to receiver including the continuous channel $h_c(t)$, A/D, D/A converters and a linear equalizer $t(n)$. The discrete time input and discrete output system shown in the shaded area of Fig. 2.3(a) can be modeled as a discrete time channel with an LTI filter $h(n)$ and additive noise $\upsilon_d(n)$ as shown in Fig. 2.3(b). Usually the discrete time channel $H(z)$ can be modeled as a rational transfer function $H(z) = P(z)/B(z)$. With proper equalization ($T(z) = B(z)$), the system in Fig. 2.3(b) can be redrawn as Fig. 2.3(c). Now we have an FIR equalized channel $P(z)$ and equalized additive noise $\upsilon(n)$. Usually, a certain redundancy is introduced to cancel ISI; the interpolation ratio $N = M + K$, where K is the number of redundancy samples. The length of the transmitting and receiving filters is also N. In the DFT based DMT transceiver,redundancy takes the form of cyclic prefix. In the DFT based DMT transceiver, redundancy takes the form of cyclic prefix. If the equalized channel $P(z)$ has order L, a cyclic prefix of length $K = L$ is sufficient for complete ISI cancellation in this case. Note that overinterpolation causes a bit rate reduction by a factor of M/N. The transmission bit rate R_b is given by

$$R_b = \frac{M}{N} f_s b, \tag{2.3}$$

where f_s is the sampling frequency and b is the average number bits allocated to the modulation symbols.

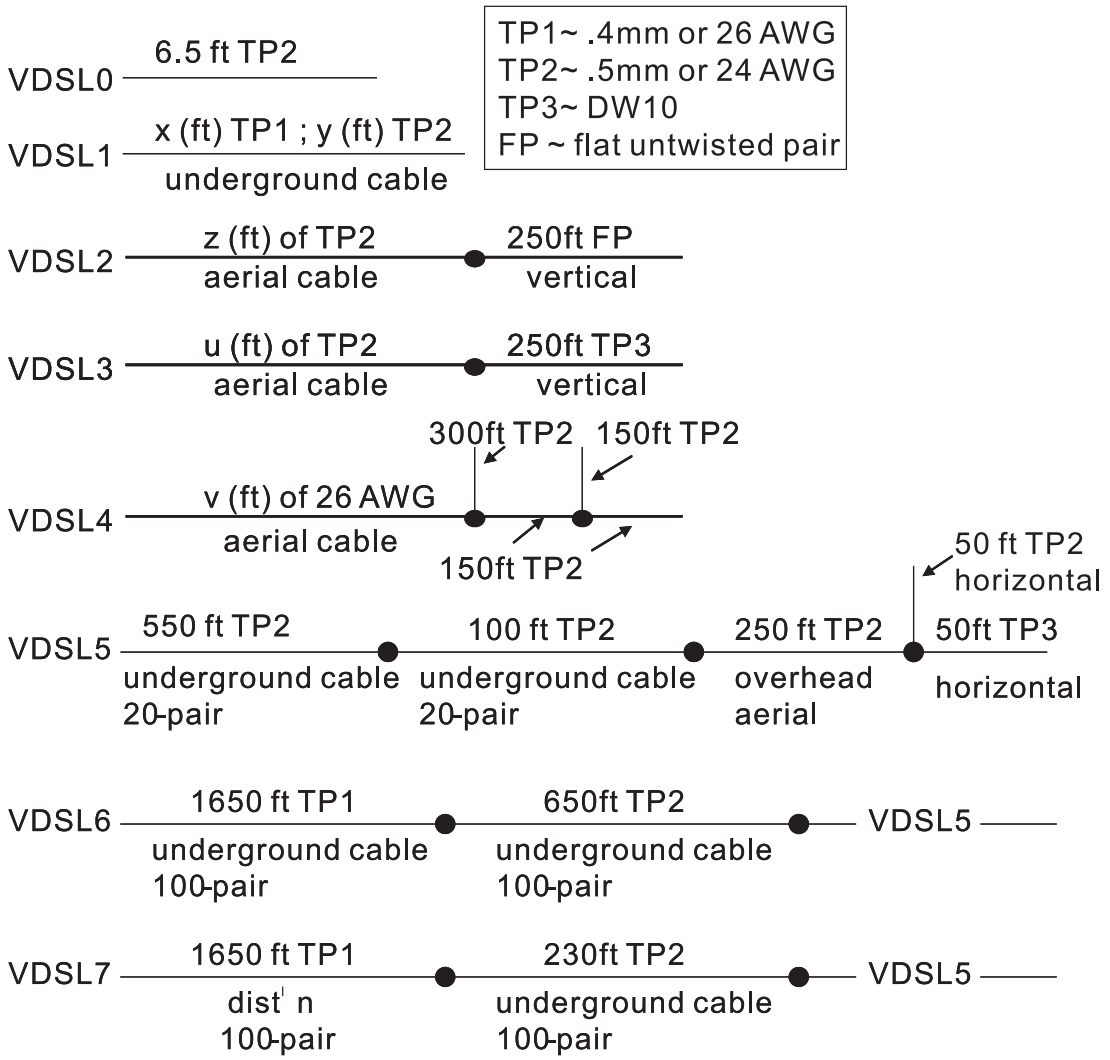

Figure 2.1: VDSL test loops

Table 2.1: VDSL test loop length

Variable Name	Short Value	Medium Value	Long Value
x (VDSL1)	1000 ft. (304.8m)	3000 ft. (914.4m)	4500 ft. (1.3716km)
y (VDSL1)	1500 ft. (457.2m)	3000 ft. (914.4m)	4500 ft. (1.3716km)
z (VDSL2)	1500 ft. (457.2m)	3000 ft. (914.4m)	4500 ft. (1.3716km)
u (VDSL3)	1500 ft. (457.2m)	3000 ft. (914.4m)	4500 ft. (1.3716km)
v (VDSL4)	1000 ft. (304.8m)	3000 ft. (914.4m)	4500 ft. (1.3716km)

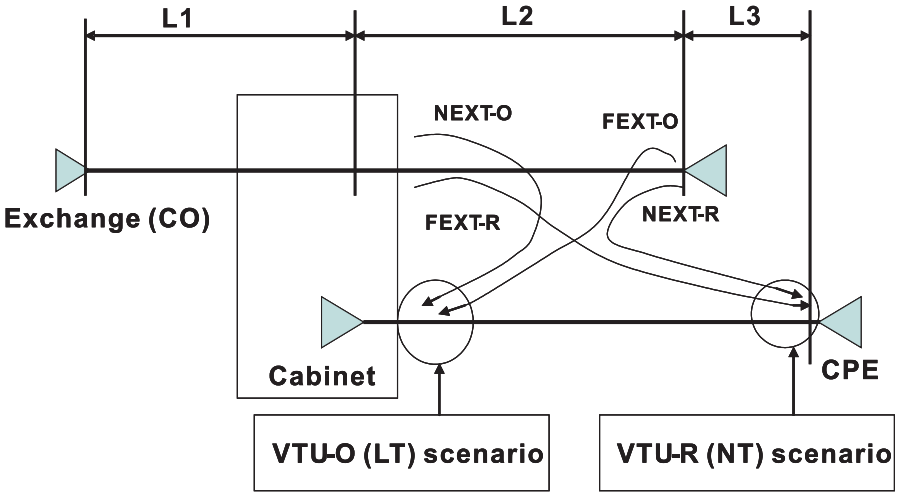

Figure 2.2: Alien crosstalk noise model definition for different scenarios

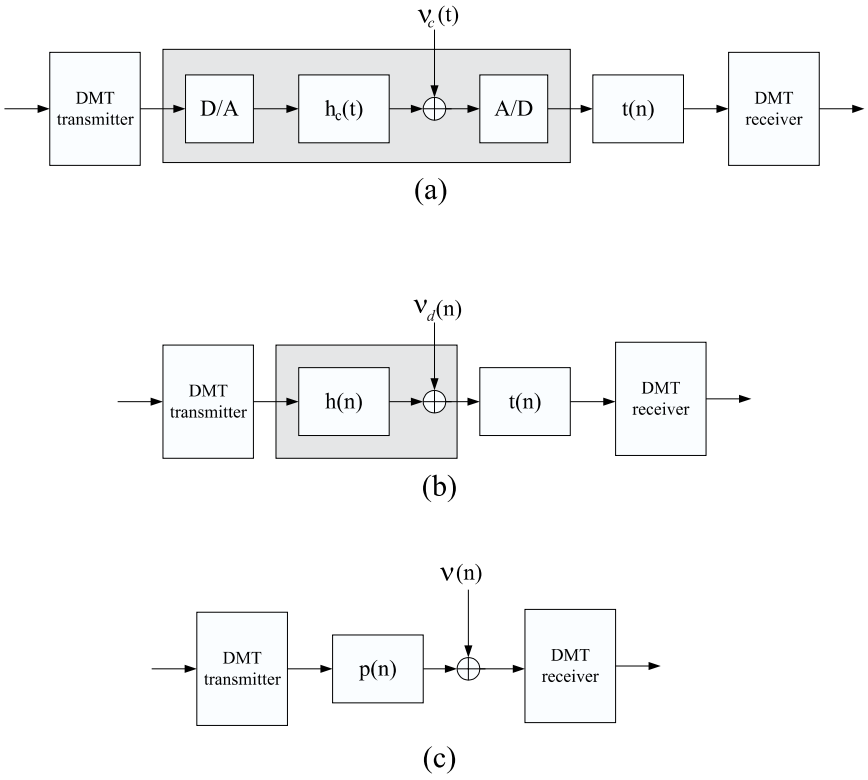

Figure 2.3: Illustration for the derivation of discrete time channel model.

Chapter 3

DFT based VDSL System

3.1 VDSL System

In this section, we will investigate the DFT based VDSL system. VDSL transceiver shall use Frequency Division Duplexing (FDD) to separate upstream and downstream transmission. The frequency plan shall consist of two upstram bands denoted as 1U, 2U and two downstream bands denoted as 1D, 2D. The bands are allocated as shown in Fig. 3.1. The values of the splitting frequencies f_i is as given in Table 3.1. From Fig. 3.1 and Tabel 3.1 we can see that the frequency band from 0.138 MHz to 12 MHz is separated into four subband, the first downstream band (1D) is started from 138 kHz and ended at 3.75 MHz, the second downstream (2D)is started from 3.75 MHz and ended at 8.5 MHz, the first upstream band (1U) is started from 3.75 MHz and ended at 5. MHz and the second upstream band (2U) is started from 8.5 MHz and ended at 12 MHz. And one optional band is allocated between 25 kHz and 138 kHz . The use of optional band shall be negotiated during the initialization to indicate if the capability exists and select one of the following options:

- Use of the band for upstream transmission;
- Use of the band for downstream transmission;
- The band is not used.

The modulation shall use a maximum number of sub-carriers equal to $N_{SC} = 2^{n+8}$, where n can take the values 0, 1, 2, 3, 4. Disjoint subsets of the N_{SC} sub-carriers shall be defined for use in downstream and upstream directions. These subsets are determined by the above frequency plan. The exact subsets of sub-carriers used to modulate data in each direction shall be determined during initialization shall be based on management system settings and the signal-to-noise ratios (SNRs) of the subchannels. In many cases the number of sub-carriers used in a direction will be less than the maximum number allowed by the partitioning. Transmission may take place on up to $N_{SC} - 1$, since DC is not used. The actual number of sub-carriers used may be lower than this maximum number. The lower limit depends on the presence of amateur radio frequency bands and the required notching in this bands, the POTS (plain old telephone service) or ISDN (integrated services digital network) splitter, PSD (power spectrum density) masks, implementation specific filters and the services to be provided.

The general DFT based VDSL system is shown in Fig. 3.2, where $M = 2N_{SC}$. Because the QAM is used to map bitstream to symbols, the symbols at the input of the transmitter will be complex number. To ensure a real-value transmit signal, we should impose the constraint on the symbols that

$$x_n = x^*_{M-n}, \quad n = 1, \cdots, M-1. \tag{3.1}$$

We may think in this way, every time we send $M/2$ symbols, including zeros for unused subchannels, for a block, after symbols symmetrization, the block will have M symbols.

Unlike the ADSL application, the redundancy in VDSL transmission system includes cyclic prefix and cyclic suffix and then windowed to reduce sidelobe energy. The last L_{CP} samples of the IDFT output shall be prepended to the $2N_{SC}$ time-domain samples as the cyclic prefix. The first L_{CS} samples shall be appended to the block of time-domain samples as the cyclic suffix. The first β samples of the prefix and last β samples of the suffix shall be used for shaping the envelope of the transmitted signal. The maximal value of β shall be 16×2^n. The windowed parts of consecutive symbols shall overlap (β samples). Fig. 3.3 summarizes all the

operations that have to be performed and illustrates the relationship between the various parameters. The total cyclic extension is defined as $L_{CE} = L_{CP}+L_{CS}-\beta$. Hence one block of time-domain samples consists of $N = 2N_{SC}+L_{CE}$. The values L_{CP}, L_{CS} and β shall be chosen in order to satisfy the equation $(L_{CP}+L_{CS}-\beta) = m \times 2^{n+1}$, where m shall be an integer value. For a given choice of the cyclic extensions and windowing length β, the symbols will be transmitted at a symbol rate equal to:

$$f_s = \frac{2N_{SC} \times \triangle f}{2N_{SC} + L_{CP} + L_{CS} - \beta}, \tag{3.2}$$

where $\triangle f$ is the tone spacing, 4.3125 kHz. L_{CP}, L_{CS} and β shall be chosen such that $L_{CP}+L_{CS}-\beta$ can at least take the value 40×2^n. If we select $L_{CE} = 40 \times 2^n$, this will results in a 4 kHz symbol rate, which is identical to ADSL symbol rate.

Because the DMT symbol has a high peak to average power ratio (PAR), peak values in the signal may be clipped by the D/A-converter. This effect approximates to an additive noise that is comparable with impulse noise (with an amplitude equal to the clipped portion, but with opposite sign). This noise will be almost white over all the subchannels. It is likely that the subchannels with the densest constellations (i.e. the tones with the largest SNR) will be more affected when this noise present since these subchannels have smaller distance between constellation points. Thus, an error is more likely to occur. If the latency can be supported, we may reorder the subchannels and apply the combination of interleaving and error control coding (ECC), RS coding in VDSL application, to these subchannels with large constellation. Thus the bitstream source x_k in Fig. 3.2 has two portions. The first one comes from the fast buffer which doesn't pass through interleaving and coding, hence no latency presents. The second part is passed through interleaving and coding, hence results in latency. In this way, the occassional errors on the subchannels with large constellations due to the clipping can be corrected by the combination of interleaving and RS coding. This is referred to tone ordering.

The signal after CP and CS extension is multiplied by a set of scalars $\{g_0, g_1, \cdots, g_{N+\beta-1}\}$ respectively, where g_i is the coefficient of the window function and then

the last β samples are overlapped to the next symbol. This system is analogous to the overlapping windowed OFDM in [8].

3.2 Filterbank Representation of DFT based VDSL Transmitter

Consider the transmitter of DFT based VDSL system as shown in Fig. 3.2, it can be transformed into an equivalent filterbank[1] as shown in Fig. 3.4 where the prototype filter $G(z) = \sum_{k=0}^{N+\beta-1} g_k z^{-k}$ and $N = M + L_{CP} + L_{CS} - \beta$.

Assume the input symbols $\{x_0, x_1, \cdots, x_{M-1}\}$ to be uncorrelated and the autocorrelation function $R_{x_k}[m] = \sigma_x^2 \delta_{m,k}$. The PSD of the k-th branch output is

$$S_{y_k}(e^{jw}) = \frac{\sigma_x^2}{N} \left| G(e^{j(w - k\frac{2\pi}{M})}) \right|^2 . \tag{3.3}$$

The overall PSD of the transmitter output can be obtained by summing up the PSDs of the subchannels,

$$S_y(e^{jw}) = \sum_{k=0}^{M-1} S_{y_k}(e^{jw}) = \frac{\sigma_x^2}{N} \sum_{k=0}^{M-1} \left| G(e^{j(w - k\frac{2\pi}{M})}) \right|^2 . \tag{3.4}$$

Assume the sampling period of DAC is T_s and the reconstruction filter is $H_r(j\Omega)$. The PSD of the signal after DAC is

$$S_{y_c}(e^{j\Omega}) = S_y(e^{j\Omega T_s}) \left| H_r(j\Omega) \right|^2 = \frac{\sigma_x^2}{N} \left| H_r(j\Omega) \right|^2 \sum_{k=0}^{M-1} \left| G(e^{j(\Omega T_s - k\frac{2\pi}{M})}) \right|^2 . \tag{3.5}$$

If the reconstruction filter is an ideal lowpass filter, it would be the form $H_r(j\Omega) = \Pi(\frac{T_s}{2\pi}\Omega)$, where

$$\Pi(\Omega) = \begin{cases} 1, & |\Omega| < \frac{1}{2}, \\ 0, & \text{otherwise.} \end{cases}$$

The PSD of the signal after DAC becomes,

$$S_{y_c}(e^{j\Omega}) = \frac{\sigma_x^2}{N} \Pi(\frac{T_s}{2\pi}\Omega) \sum_{k=0}^{M-1} \left| G(e^{j(\Omega T_s - k\frac{2\pi}{M})}) \right|^2 . \tag{3.6}$$

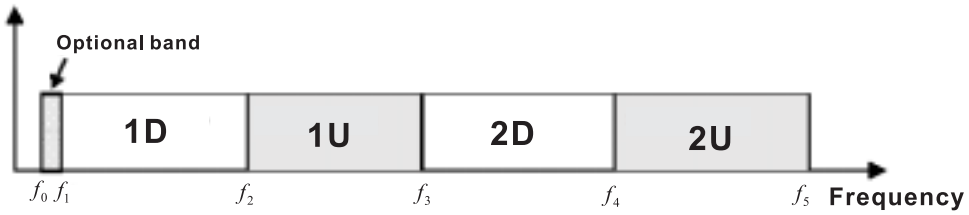

Figure 3.1: VDSL band allocation

Table 3.1: VDSL band separating frequencies

Separating Frequencies	f_0	f_1	f_2	f_3	f_4	f_5
(Mhz)	0.25	0.138	3.75	5.2	8.5	12

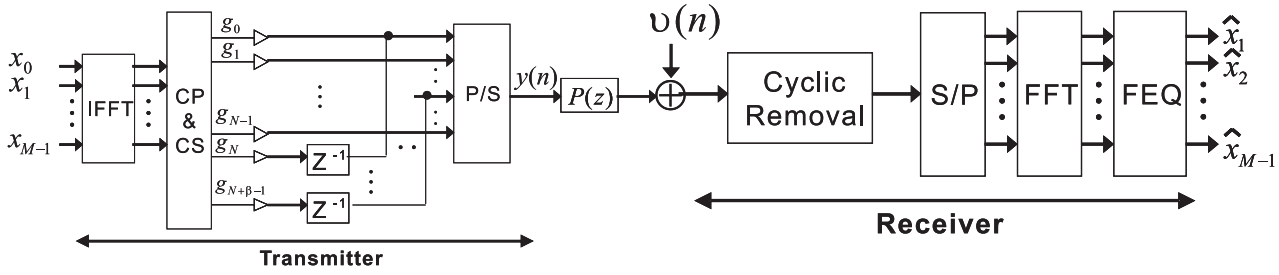

Figure 3.2: Block diagram of DFT based VDSL system

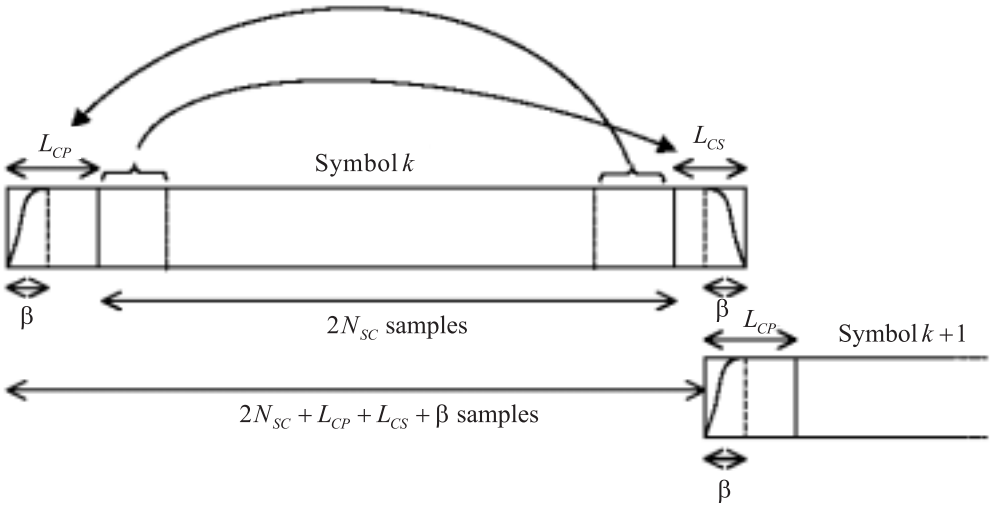

Figure 3.3: Cyclic extensions, windowing and overlap of DMT symbols.

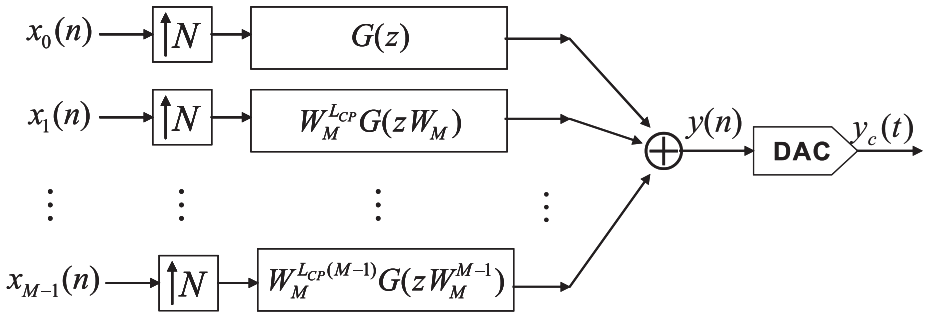

Figure 3.4: Filterbank representation of the DFT based VDSL transmitter.

Chapter 4

Optimal Power Allocation

In this chapter, we will study two methods of power allocation, conventional water-filling and optimal power allocation. Conventional water-filling power allocation does not constrain on the minimum non-zero power allocated to subchannels. Some tones will be allocated power that is not sufficient to transmit any bit, given the desired probability of error. In this case, the powr allocated to these subchannels will be wasted. However, optimal power allocation method distributes power to subchannel according to its condition, if the power allocated to the subchannel is not sufficient to transmit any bit, we will turn off this subchannel. Obviously, optimal power allocation method can fully utilize the power to improve the bit number carried by each subchannel. Fig. 4.2 and 4.3 show the downstream and upstream power spectrum density template for fiber-to-the-exchange (FTTEx) scenario, respectively. Let $G(f)$ be the function determines the template in the figures. Then the total power P under the template is given by

$$P = \int_{-\infty}^{\infty} G(f)df, \tag{4.1}$$

and the maximum power can be allocated to each subchannel is limited by the template. Let the maximum power can be allocated to the kth subchannel be $P_{k,max}$.

4.1 Water-filling Power Allocation

For a set of M parallel subchannels as shown in Fig. 1.2, to maximize the data rate R_b is equivalent to maximize the achievable total bits

$$b = \sum_{k=0}^{M-1} \frac{1}{2} \log_2(1 + \frac{P_k}{\Gamma N_k}), \tag{4.2}$$

where Γ is the SNR gap determined by the symbol error rate. N_k is a fixed function of the channel, but P_k can be varied to maximize b, subject to the total power constraint that

$$\sum_{k=0}^{M-1} P_k = P_{total}. \tag{4.3}$$

Using Lagrange multipliers, the cost function to maximize (4.2) subject to the constraint in (4.3) becomes

$$\frac{1}{2\ln(2)} \sum_{k=0}^{M-1} \ln(1 + \frac{P_k}{\Gamma N_k}) + \lambda(\sum_{k=0}^{M-1} P_k - P_{total}). \tag{4.4}$$

Differentiating with respect to P_k produces

$$\frac{1}{2\ln(2)} \frac{1}{P_k + \Gamma N_k} = -\lambda. \tag{4.5}$$

Thus, (4.2) is maximized, subject to (4.3), when

$$P_k + \Gamma N_k = \text{constant}. \tag{4.6}$$

The solution is known as "water-filling" solution because one can construe the solution graphically be thinking of the curve of ΓN_k as being filled with power (water) to a constant line. Fig. 4.1 shows the discrete equivalent of water-filling for a set of 6 subchannels. Note in Fig. 4.1 that 4 of the six subchannels have positive powers, while 2 were eliminated for having negative power, or equivalently having a noise power that exceeded the constant line of water filling. The conventional water-filling solution only has the constraint on the total power. Since the applications in VDSL system have transmitting power spectrum template as given in Fig. 4.2 and 4.3, it gives the maximum power constraint on each subchannel. Thus, if we want to use the water-filling solution in (4.6), denoting

the solution as $\{P_{0,water}, P_{1,water}, \cdots, P_{M-1,water}\}$, we need to do follows after the water-filling procedure:

$$P_k = \min(P_{k,water}, P_{k,max}), \quad k = 0, 1, \cdots, M-1. \tag{4.7}$$

Although the solution given in (4.7) can meet the maximum power constraint, the excess power, $P_{k,water} - P_{k,max}$, for the kth subchannel which has allocated power larger than maximum power $P_{k,max}$ is not utilized at last. The solution also has no constraints on the non-zero power. When the non-zero power is not sufficient to transmit any bit, the power will go wasted. Thus in the next section, we will introduce the optimal power allocation to settle this problem.

4.2 Optimal Power Allocation Method

In order to fully utilize the usable power, we want the power allocated to a subchannel is large enough to transmit a bit. Thus we add a constraint on the minimum power, $P_{k,min}$ for the kth subchannel. The power allocated to kth subchannel needs not to less than $P_{k,min}$ or we will turn off it.

The problem we want to solve is that for the equivalent DFT based DMT system shown in Fig. 1.2, given the noise power N_k for the kth subchannel and assume the desired symbol error rate for each subchannel to be the same, find the power allocated to it to maximize the total bits in (4.2), subject to the total power constraint (4.3) and $P_{kmin} \leq P_k \leq P_{k,max}$ or $P_k = 0$, where M is the number of total usable subchannels and Γ is the SNR gap determined by the symbol error rate.

We can solve it by using the method of Lagrange multipliers with inequality[10]. For this, we construct the Lagrange function L as

$$L = \sum_{k=0}^{M-1} \frac{1}{2} \log_2(1 + \frac{P_k}{\Gamma N_k}) + \lambda(\sum_{k=0}^{M-1} P_k - P_{total}) + \sum_{k=0}^{M-1} \mu_k P_k + \sum_{k=0}^{M-1} \nu_k (P_{k,max} - P_k), \tag{4.8}$$

where λ, μ_k and ν_k are the Langrange multipliers.

The Kuhn-Tucker conditions are given by

$$\frac{\partial L}{\partial P_k} = 0, \quad k = 0, 1, \cdots, M-1$$

$$\begin{aligned}
\mu_k P_k = 0, \quad & k = 0, 1, \cdots, M-1 \\
\nu_k (P_{k,max} - P_k) = 0, \quad & k = 0, 1, \cdots, M-1 \\
0 \le P_k \le P_{k,max}, \quad & k = 0, 1, \cdots, M-1 \\
\mu_k, \nu_k \ge 0, \quad & k = 0, 1, \cdots, M-1
\end{aligned} \tag{4.9}$$

1. If $0 < P_k < P_{k,max}$, from (4.9), the constraint on the kth subchannel are inactive and $\mu_k = \nu_k = 0$. Hence, we have

$$\frac{\partial L}{\partial P_k} = \frac{1}{2 \ln 2} \frac{1}{P_k + \Gamma N_k} + \lambda = 0 \tag{4.10}$$

or

$$P_k = c - \Gamma N_k, \tag{4.11}$$

where $c = -\frac{1}{2\lambda \ln 2}$.

2. If $P_k = 0$, from (4.9), the constraint $P_k \le P_{k,max}$ is inactive and $\mu_k \ge 0, \nu_k = 0$. Hence, we have

$$\frac{\partial L}{\partial P_k} = \frac{1}{2 \ln 2} \frac{1}{P_k + \Gamma N_k} + \lambda + \mu_k = 0 \tag{4.12}$$

or

$$P_k \ge c - \Gamma N_k. \tag{4.13}$$

3. If $P_k = P_{k,max}$, from (4.9), the constraint $P_k \ge 0$ is inactive and $\mu_k = 0, \nu_k \ge 0$. Hence, we have

$$\frac{\partial L}{\partial P_k} = \frac{1}{2 \ln 2} \frac{1}{P_k + \Gamma N_k} + \lambda - \nu_k = 0 \tag{4.14}$$

or

$$P_k \le c - \Gamma N_k. \tag{4.15}$$

From 1,2 and 3, we have

$$P_k = \begin{cases} c - \Gamma N_k, & P_{k,min} \le c - \Gamma N_k < P_{k,max} \\ 0, & c - \Gamma N_k < P_{k,min} \\ P_{k,max}, & c - \Gamma N_k \ge P_{k,max} \end{cases} \tag{4.16}$$

In the above derivation, we need to solve for the Lagrange multipliers λ, μ_k and ν_k. To find out the solutions may be difficult, especially when M is large. Hence, we appeal to the conventional water-filling optimization. In order to fully utilize the usable power, we substitute the lower bound $P_{k,min}$ for 0 in the original method. $P_{k,min}$ is decided to ensure the subchannel that is allocated power is able to carry a bit. If the power allocated to the kth subchannel is less than the lower bound $P_{k,min}$, then we turn off this subchannel and distribute the power to other usable subchannels.

To maximize (4.2) using water-filling optimization, we have

$$\begin{aligned} P_0 + \Gamma N_0 &= K \\ P_1 + \Gamma N_1 &= K \\ &\vdots \\ P_{M-1} + \Gamma N_{M-1} &= K \\ P_0 + P_1 + \cdots + P_{M-1} &= P_{total}, \end{aligned} \tag{4.17}$$

where K is a constant. Or

$$\begin{aligned} K &= \frac{1}{M}(P_{total} + \Gamma \sum_{k=0}^{M-1} N_k) \\ P_k &= K - \Gamma N_k, \quad k = 0, 1, \cdots, M-1 \end{aligned} \tag{4.18}$$

If the solution to the kth subchannel in (4.18) is less than $P_{k,min}$, we turn off it. Until there is no subchannel's power less than its lower bound, we check if there is any subchannel's power is larger than its upper bound. If the kth subchannel's power larger than its upper bound $P_{k,max}$, we set its power as $P_{k,max}$ and distribute the excess power, $P_k - P_{k,max}$, to other usable subchannels.

The procedure to do the optimal power allocation is given as follows:

1. Solve the power allocated to each subchannel using conventional water-filling optimization method.

2. Sort subchannel such that $P_{0,max} + \Gamma N_0 \leq P_{1,max} + \Gamma N_1 \leq \cdots \leq P_{N^*,max} + \Gamma N_{N^*}$.

3. If $P_0 \geq P_{0,max}$?

   If yes,

   (a) if $P_{0,max} < P_{0,min}$, $P_0 = 0$;

   (b) else $P_0 = P_{0,max}$;

   set $P_{total} = P_{total} - P_0$ and eliminate this subchannel, go to step 1; otherwise continue.

4. Unsort subchannel. End.

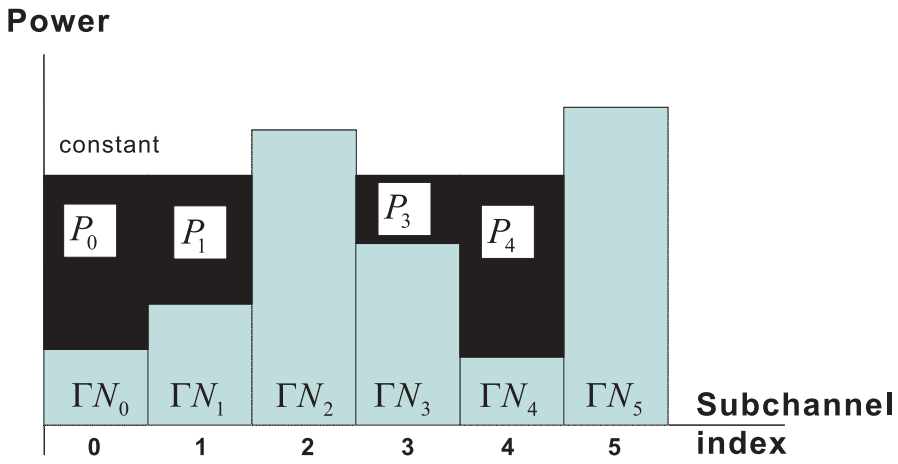

Figure 4.1: Illustration of discrete water-filing for 6 subchannels.

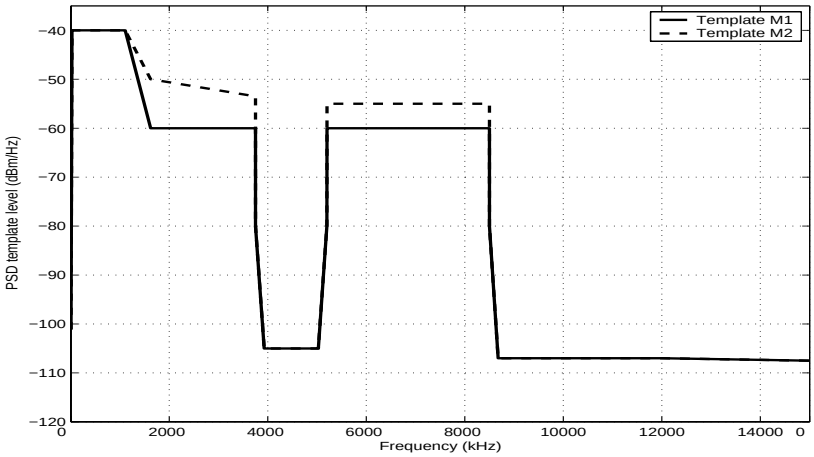

Figure 4.2: VDSL downstream templates-FTTEx

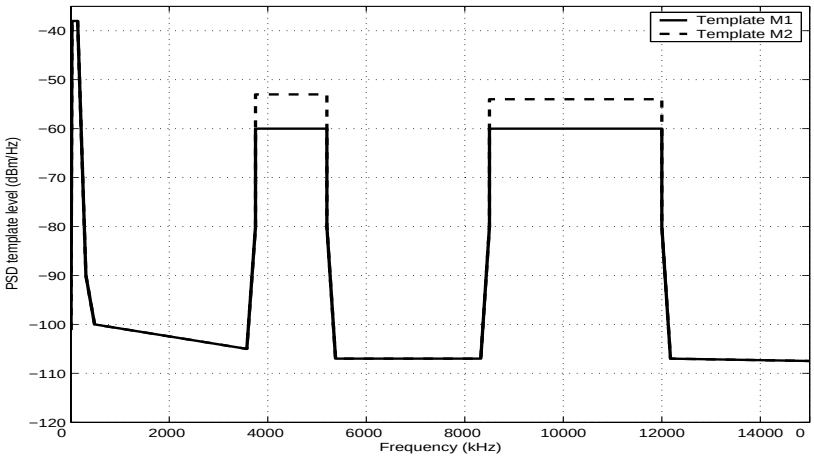

Figure 4.3: VDSL upstream templates-FTTEx

Chapter 5

Performance Evaluation

In this chapter, we will study the performances of the water-filling power allocation and optimal power allocation. We will give some discussions in this chapter. And in the end of this chapter, we will propose one method to feedback the power allocation information to the transmitter.

5.1 Simulation Result

In our simulations, we assume the maximum of sub-carrier N_{SC} 4096, cyclic extension (samples) L_{CE} 640, cyclic prefix (samples) L_{CP} 600 and β 128 samples. The maximum number of bit, b_{max}, can be allocated to each subchannel is 15. For the desired symbol error rate (SER) for each subchannel to be 10^{-4}, we set the gap be 7.3899 dB. Thus $P_{k,min}$ is determined by N_k + 7.3899 (dB). The crosstalk noise coupling coefficients for category-5 twisted-pair wire are used. The optional band is used both for downstream and upstream.The PSD profile Model A of alien noise spectra is used. In order to examine the effect of the different power allocation methods on the data rate, we use the system given in Fig. 3.2 and three arbitrary artificial loops. The test loop 1, 2 and 3 are cut from the short VDSL1, VDSL7 and VDSL4 with loop length 2km, to avoid ISI and multiplied a window to smoothen their frequency spectra. Then we will study the results using the test loops given in [5].

Fig. 5.1, Fig. 5.2 and Fig. 5.3 show the magnitude response and noise PSD associated to these three artificial channels. Fig. 5.4, Fig. 5.5 and Fig. 5.6 show

the power and Fig. 5.7, Fig. 5.8 and Fig. 5.9 show the bit allocated to the artificial channels for downstream, respectively. Fig. 5.10 and Fig. 5.11 show the power and Fig. 5.12 and Fig. 5.13 show the bit allocated to the artificial channels for upstream, respectively. Table 5.1, 5.3, 5.2 and 5.4 are the data rate for these three test loops.

The results for standard test loops are given in Table 5.5, Table 5.6, Table 5.7 and Table 5.8,. The Fig. 5.14 and Fig. 5.15 show the loop length and data rate both for downstream and upstream.

5.2 Discussion

- From the noise PSD figures, shown in Fig. 5.1(b)(c), Fig. 5.2(b)(c) and Fig. 5.3(b)(c), we can see that the most noise power is dominated by the AWGN in the used frequency bands, hence it is quite "flat" in these bands. Since the implementation of FEQ, the relative noise power magnitude in the used band is determined by the channel's magnitude response. The severer the attenuation of channel, the larger the noise power is.

- In Fig. 5.1(a), we can see the attenuation of test loop1 is moderate both in the first and second bands for both downstream and upstream. This will result in little noise enhancement. Thus we can expect the power allocated to these subchannels approximate equally, since the noise power is small relative to the allocated power. When the power is equally distributed to each subchannel, the power allocated to each subchannel will larger than -60 dBm both for downstream and upstream. Since we have maximum power constraint -60 dBm on high frequency band when Template M1 is used, the power allocated to these subchannel will be clipped as we can see in Fig. 5.4. However, when Template M2 is used, this will not happen because we have larger maximum power constraint on high frequency band as we can see in Fig. 5.5.

- The power allocation for test loop 1 will be clipped when Template M1 is

used. When the optimal power allocation is employed, we will distribute the excess power to other usable subchannels. Thus from Fig. 5.4 we can see that the power allocated to low frequency using optimal power allocation is larger than that using water-filling power allocation. This results in that the bits allocated to the low frequency subchannel (tone index less than 400) using optimal power allocation is larger than that using water-filling power allocation. The bit allocation is shown in Fig. 5.7.

- From Fig. 5.6 and Fig. 5.9, since we add the minimum power constraint for optimal power allocation, the subchannels with index larger than 900 are not allocated power; however they are allocated power when water-filling power allocation is employed. Fig. 5.9(a) shows the bit allocation for water-filling power allocation, we can see that the power allocated to subchannels with index larger than 900 is not sufficient to transmit any bit. Thus power allocated to these subchannels is wasted.

- From Fig. 5.5 we can see that the maximum power constraints are inactive for test loop 1 when Template M2 is used regardless of which power allocation method is used. This result in the same bit allocation as we can see in Fig. 5.8.

- From Fig. 5.2(a) and Fig. 5.3, since the attenuation on the high frequency band of test loop 3 is severer than that of test loop 2. These subchannels of test loop 3 will have smaller SNR. Thus these subchannels will be turned off and the power will mainly distribute to the low frequency subchannels as we can see in Fig. 5.6, Fig. 5.10 and Fig. 5.11.

- Since the subchannels allocated at high frequency band have bad condition, these subchannels will be turned off. Especially for upstream, the first and second upstream bands can not be used. Thus the power is usable when it allocated to optional band as in Fig. 5.10 and Fig. 5.11.

- Fig. 5.12 and Fig. 5.13 show the bit allocations of test loop 2 and test loop 3 for upstream. In Fig. 5.12, even though the power allocated to the optional

band using optimal power allocation is larger than that using water-filling power allocation, the improvement on date rate is limited since we have the maximum bit constraint. Since the power allocations of test loop 3 are the same for optimal and water-filling power allocation, this results in the same performance.

- From the Tables, Fig. 5.14 and Fig. 5.15, we can see that optimal power allocation outperforms the water-filling power allocation for long loop downstream when Template M1 is used; others will have the similar performance. The benefits optimal power allocation can get are: 1. the lower bound constraint $P_{k,min}$ such that the power will not wasted when the power is not sufficient to transmit any bit; 2. the excess power is distributed to other usable subchannels, thus we can fully utilize the usable power.

5.3 Payload for Optimal Power Allocation

When we use the optimal power allocation method, the information about how to allocate the power is needed for the transmitter. Hence we propose one method to do this. We group the power of subchannels first. Define g_{var} and g_{number} as the variation and maximum tone number of a group. After the power allocation in Sec. 4.2, arrange the subchannels according to their tone index. Take the first tone as the pilot one, marking its power as P_{pilot} and examine whether the power of sequential subchanels within the variation g_{var} relative to P_{pilot} or not. If yes, i.e. $P_{pilot} - g_{var} \leq power \leq P_{pilot} + g_{var}$, and the tone number of this group is less than g_{number}, group this subchannel under the current group. Otherwise, make a new group and this subchannel as pilot subchannel. At last, we transmit the total group number and g_{var}, g_{number} for each group to the transmitter.

Table 5.9, 5.10, 5.11 and 5.12 show some examples of grouping. The entries given in the table is in the form x/y which x means result data rate and y total group number. As we can expect that larger g_{number} and g_{var}, smaller the group number is. From this experiment, we can see we might have some loss on data rate after grouping.

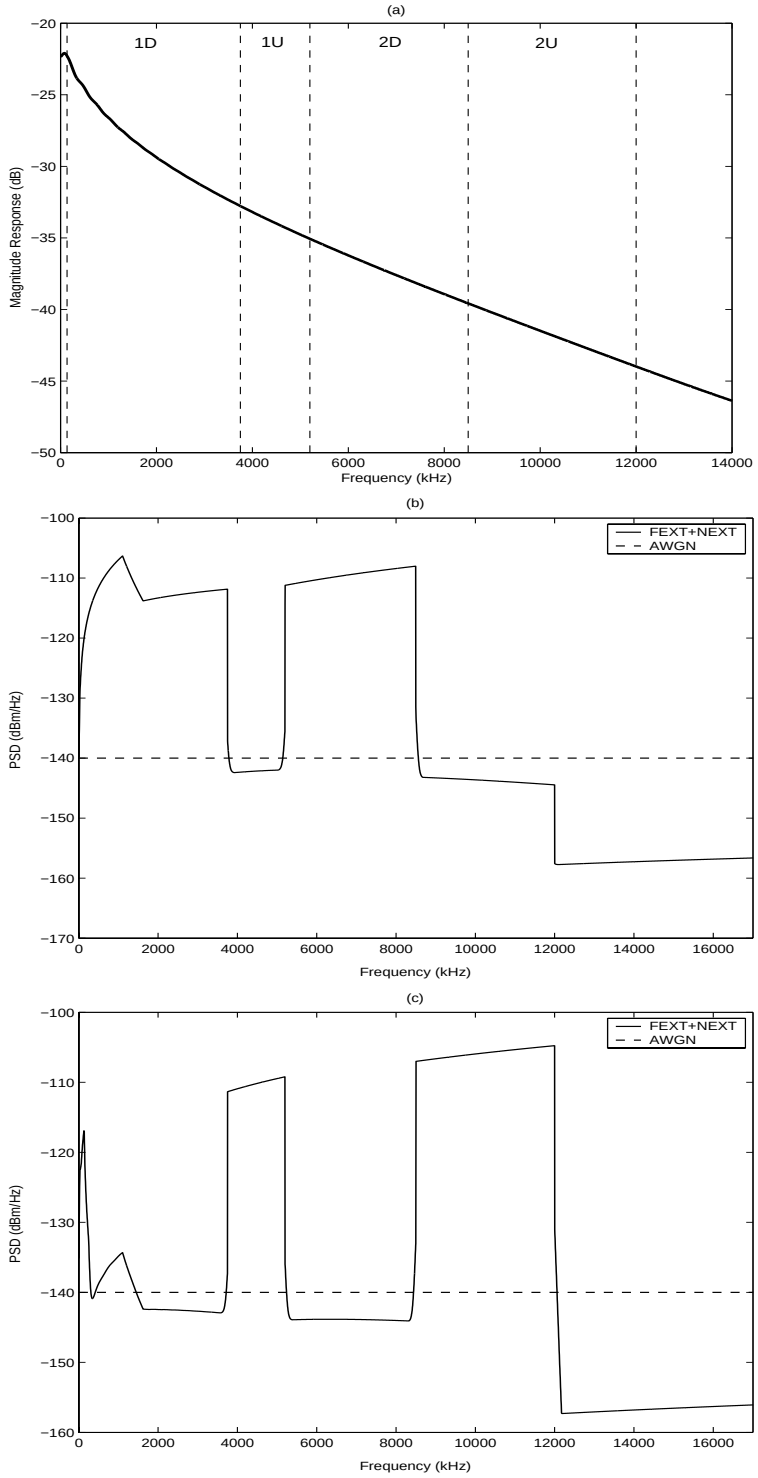

Figure 5.1: (a) Magnitude response of test loop 1; (b) Noise PSD for upstream and (c) Noise PSD for downstream (category-5 twisted pair).

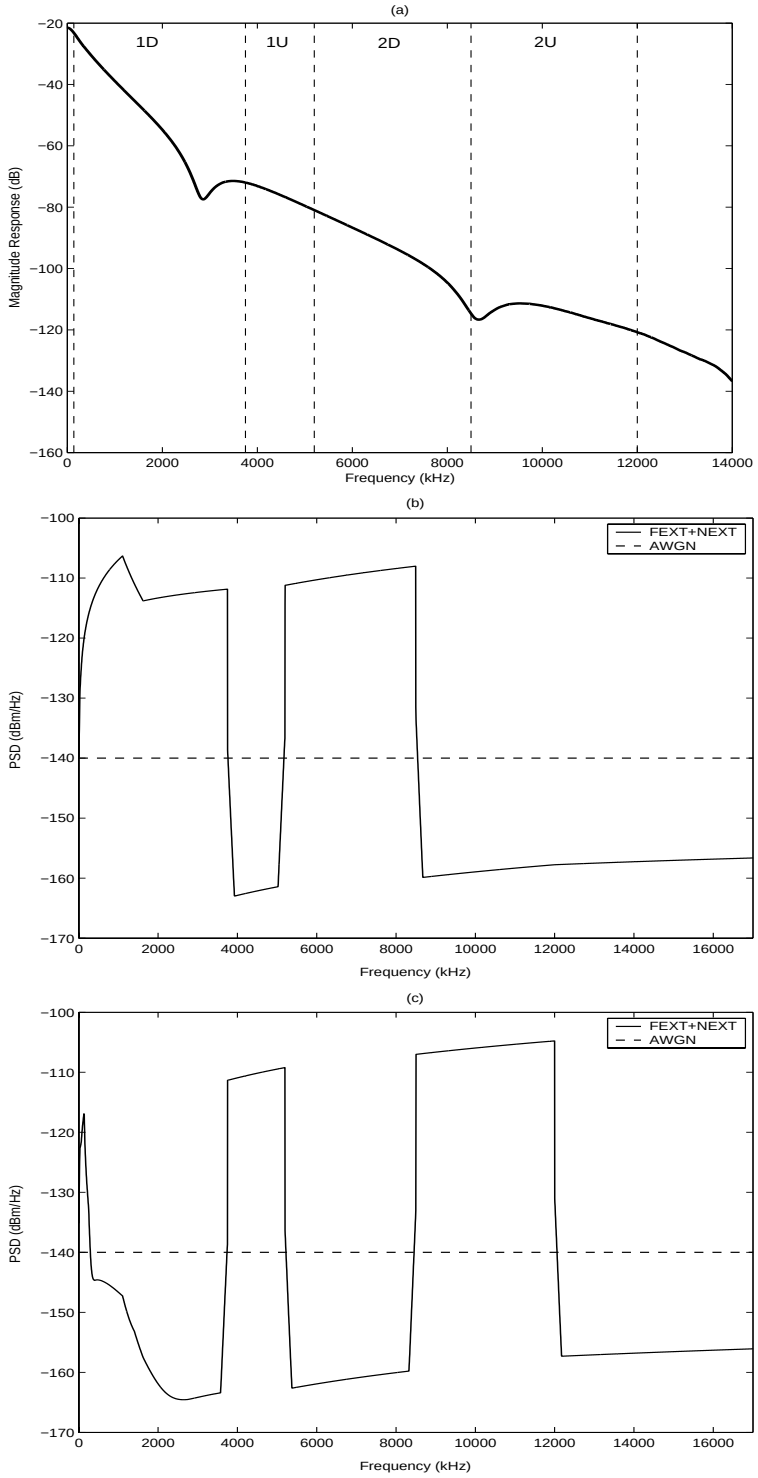

Figure 5.2: (a) Magnitude response of test loop 2; (b) Noise PSD for upstream and (c) Noise PSD for downstream (category-5 twisted pair).

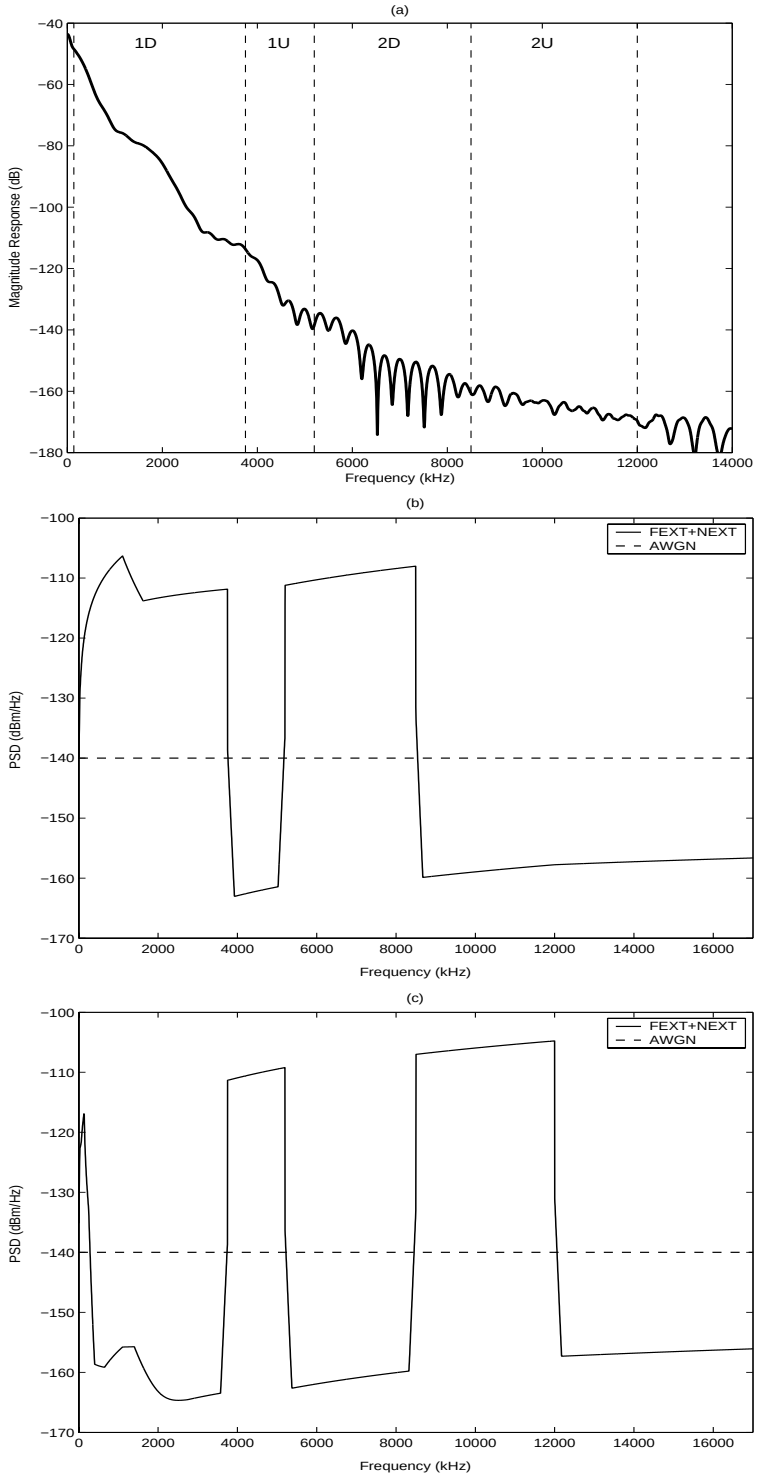

Figure 5.3: (a) Magnitude response of test loop 3; (b) Noise PSD for upstream and (c) Noise PSD for downstream (category-5 twisted pair).

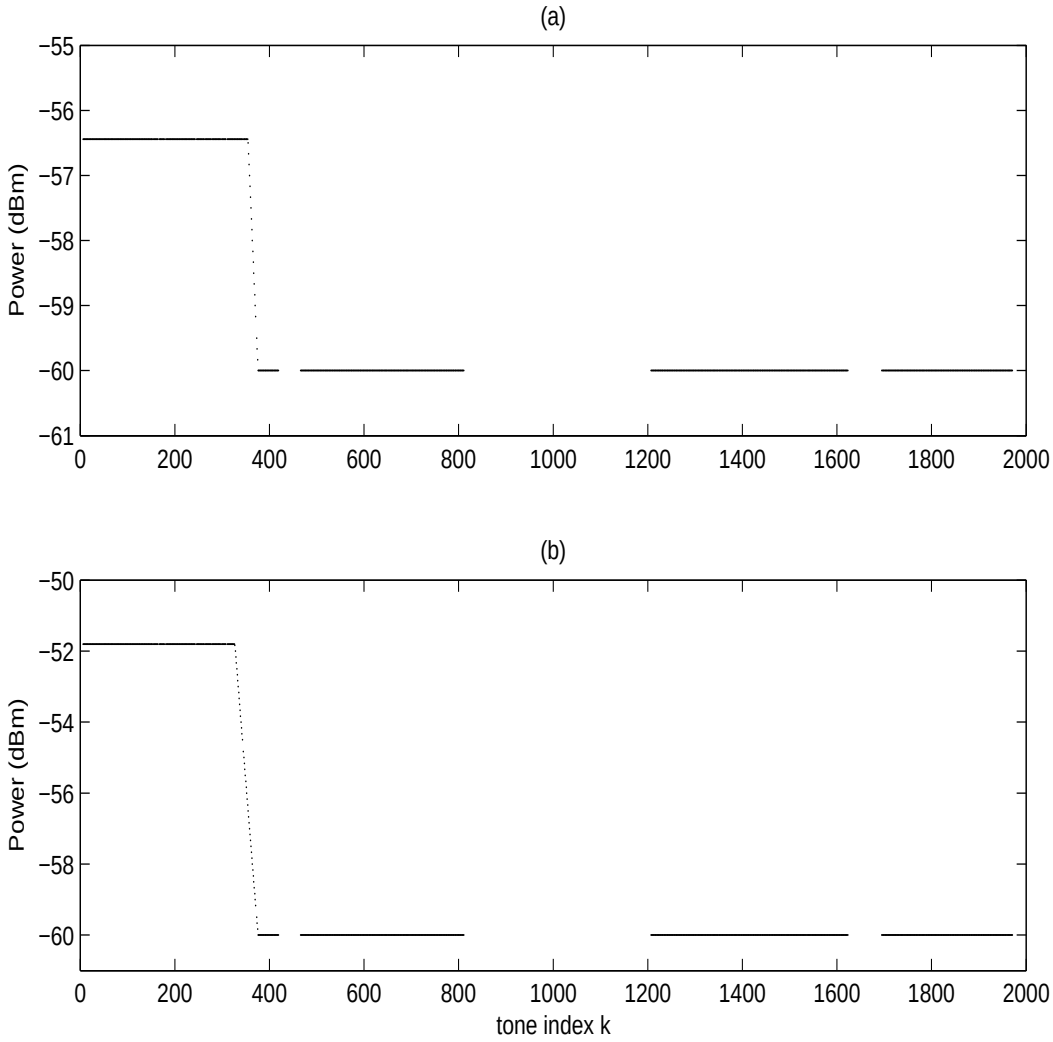

Figure 5.4: Power allocated to test loop 1 for downstream and Template M1 is used: (a) water-filling power allocation; (b) optimal power allocation.

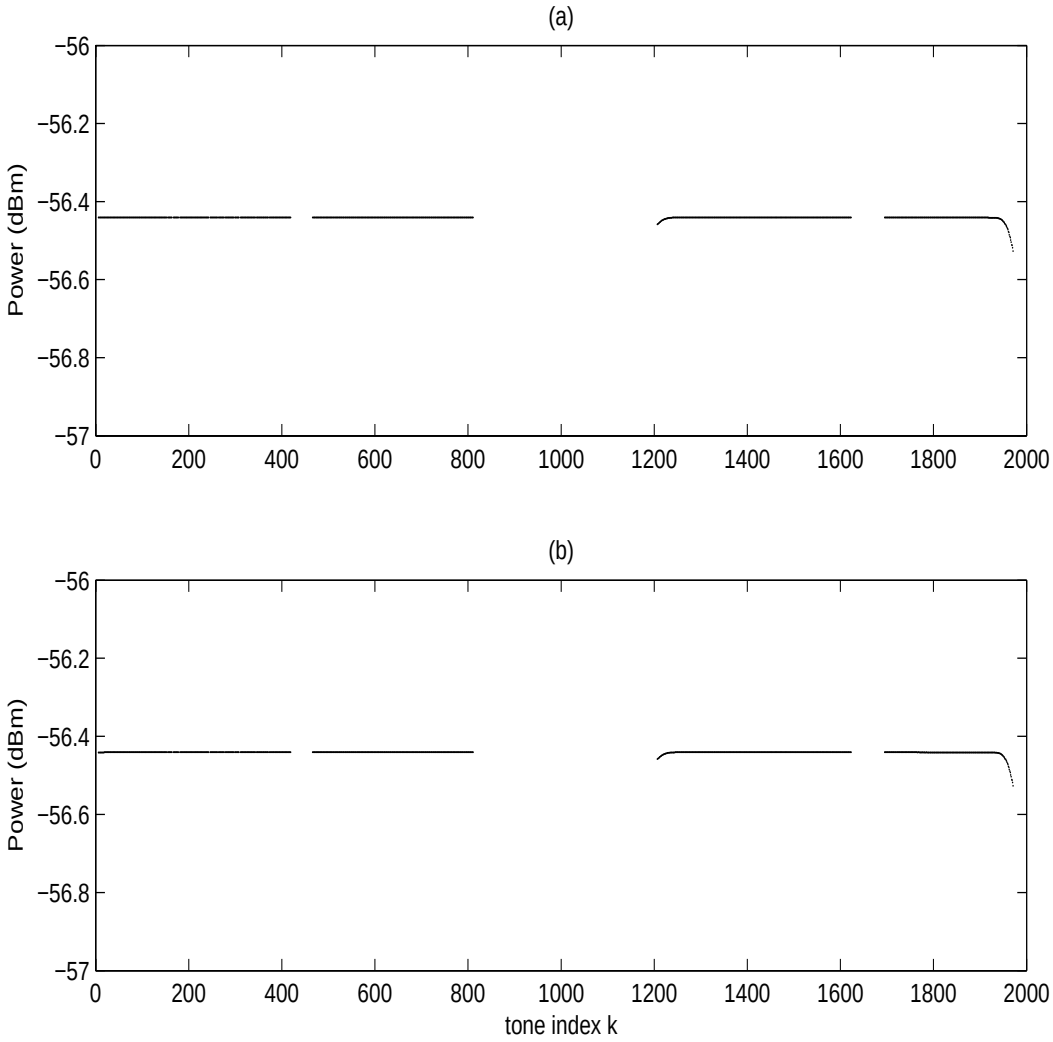

Figure 5.5: Power allocated to test loop 1 for downstream and Template M2 is used: (a) water-filling power allocation; (b) optimal power allocation.

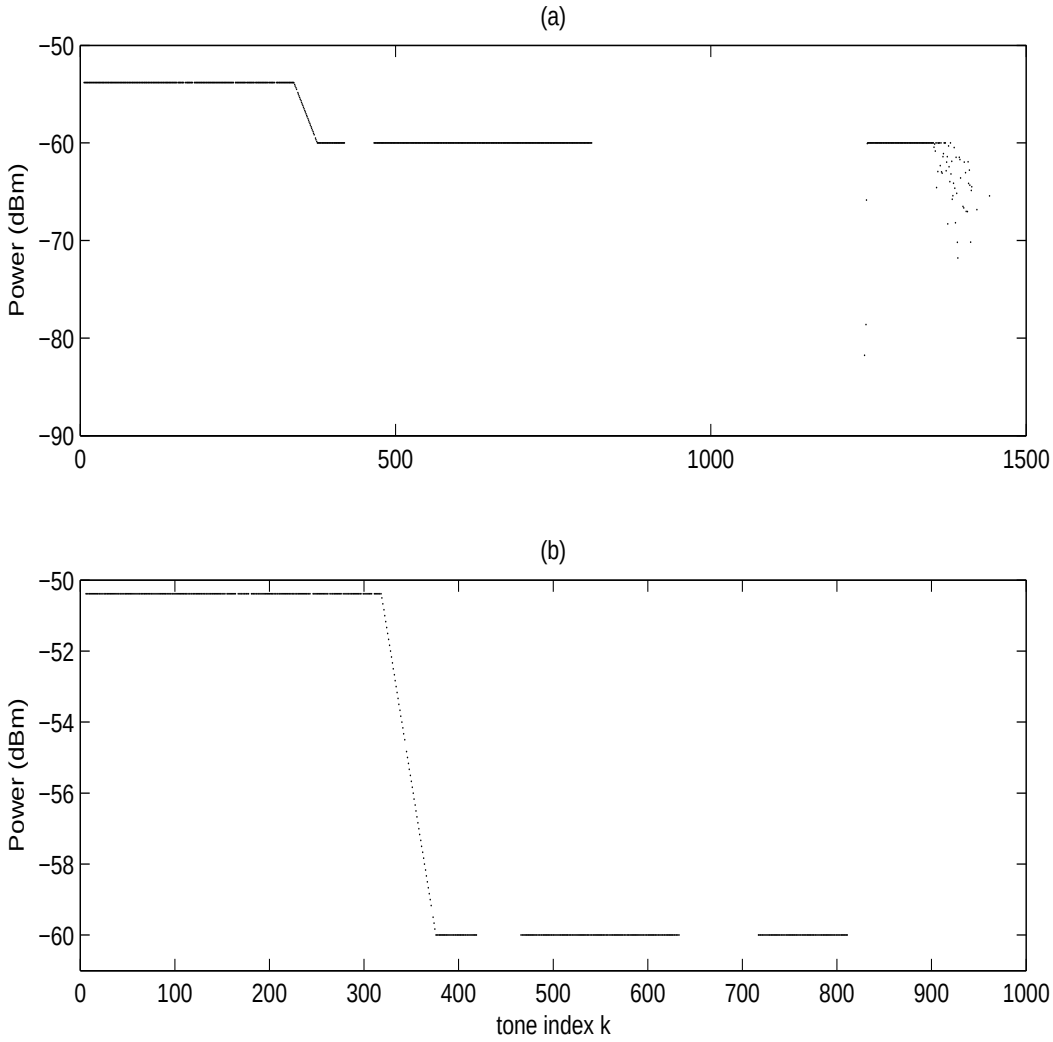

Figure 5.6: Power allocated to test loop 2 for downstream and Template M1 is used: (a) water-filling power allocation; (b) optimal power allocation.

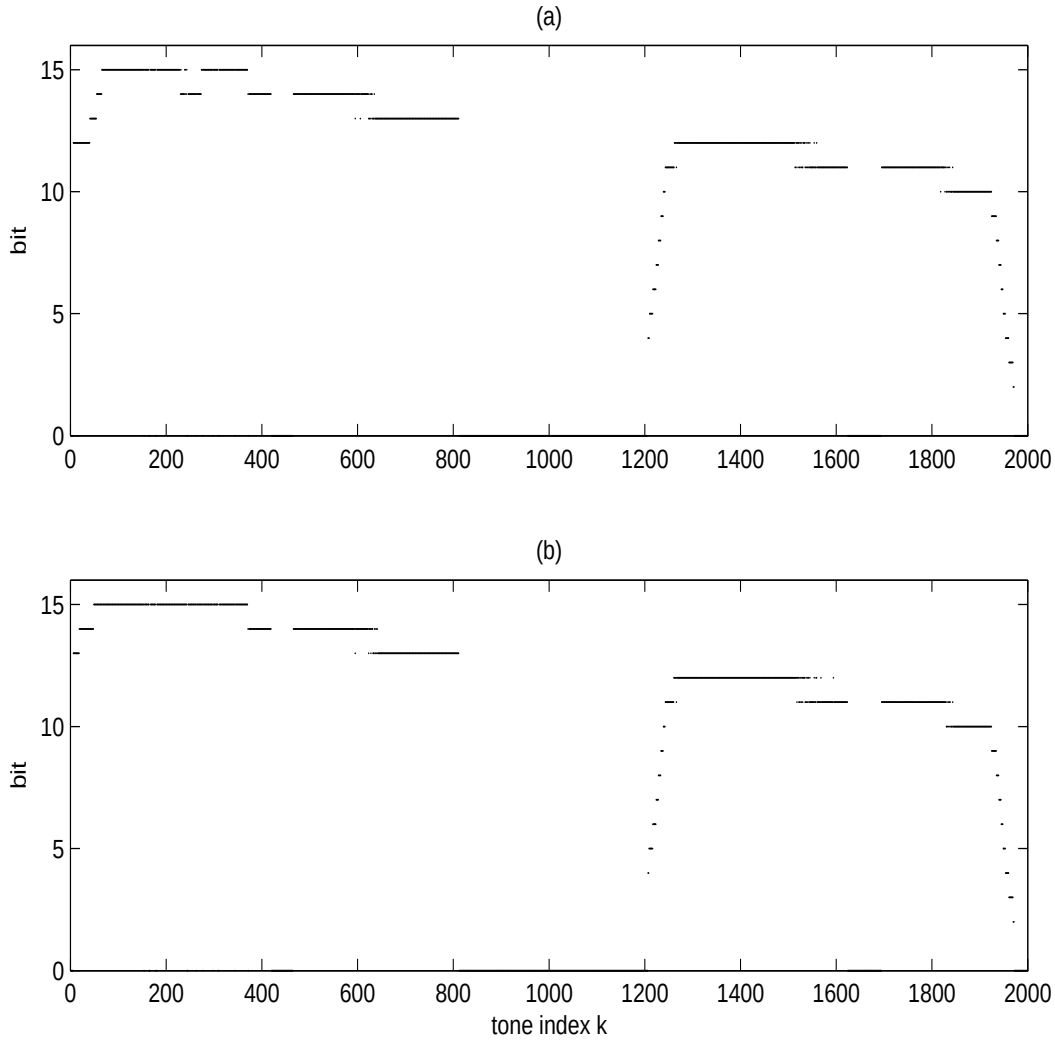

Figure 5.7: Bit allocated to test loop 1 for downstream and Template M1 is used: (a) water-filling power allocation; (b) optimal power allocation.

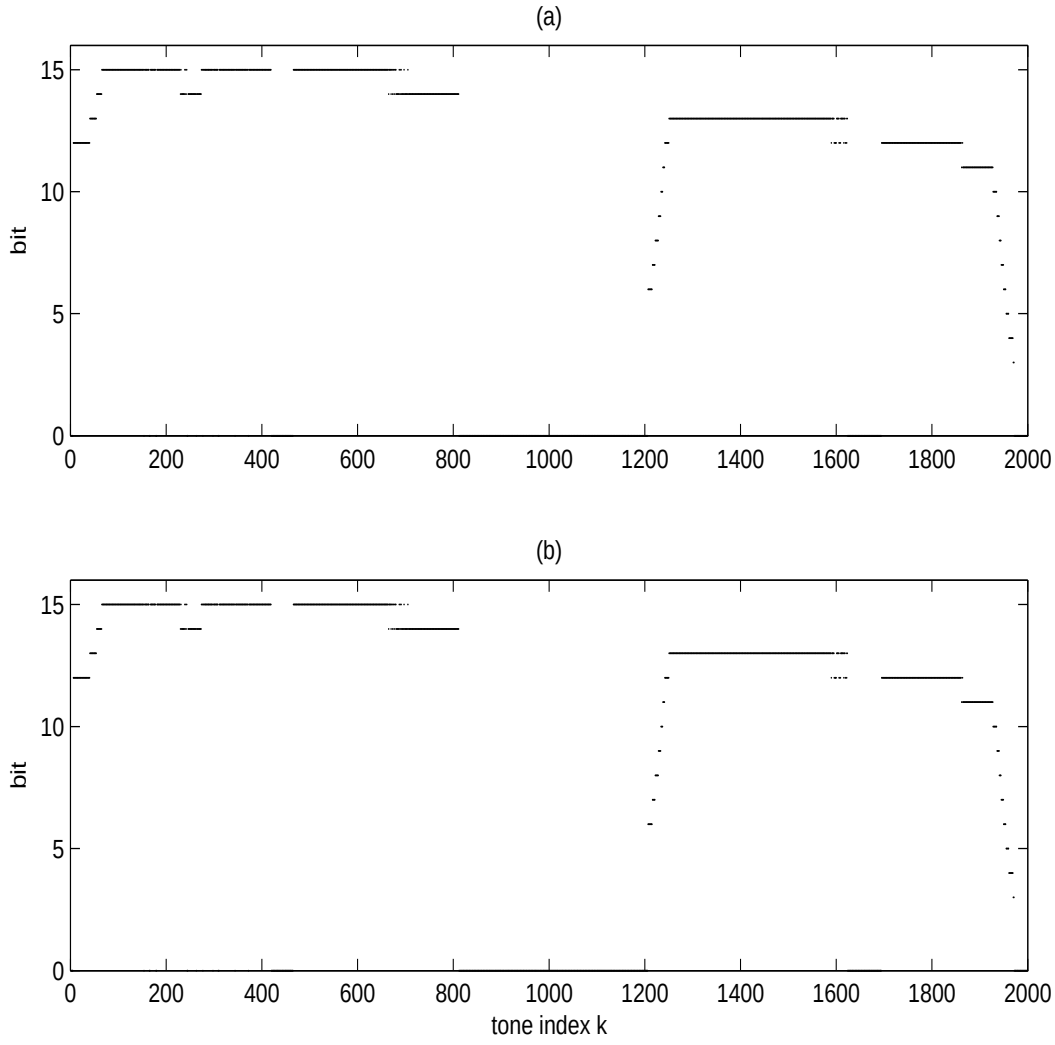

Figure 5.8: Bit allocated to test loop 1 for downstream and Template M2 is used: (a) water-filling power allocation; (b) optimal power allocation.

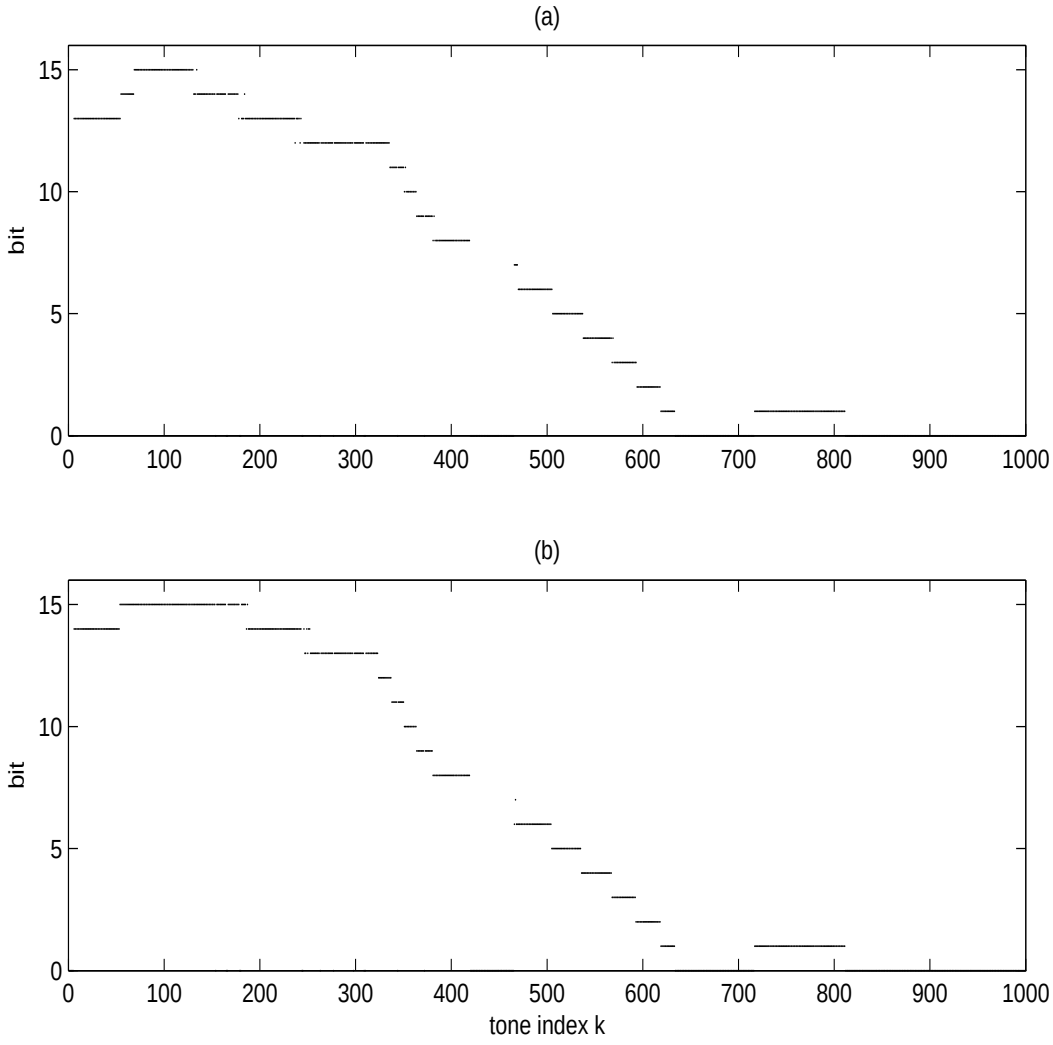

Figure 5.9: Bit allocated to test loop 2 for downstream and Template M1 is used: (a) water-filling power allocation; (b) optimal power allocation.

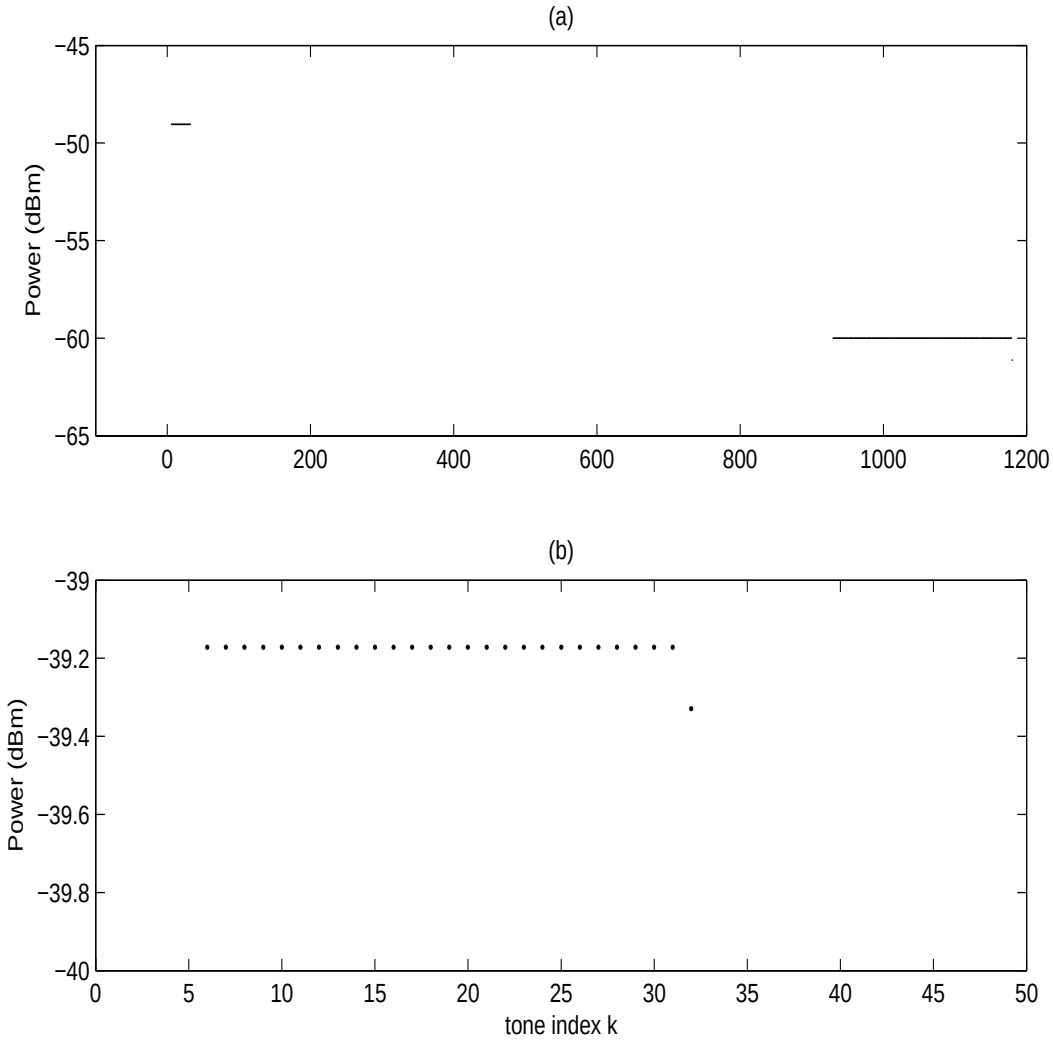

Figure 5.10: Power allocated to test loop 2 for upstream and Template M1 is used: (a) water-filling power allocation; (b) optimal power allocation.

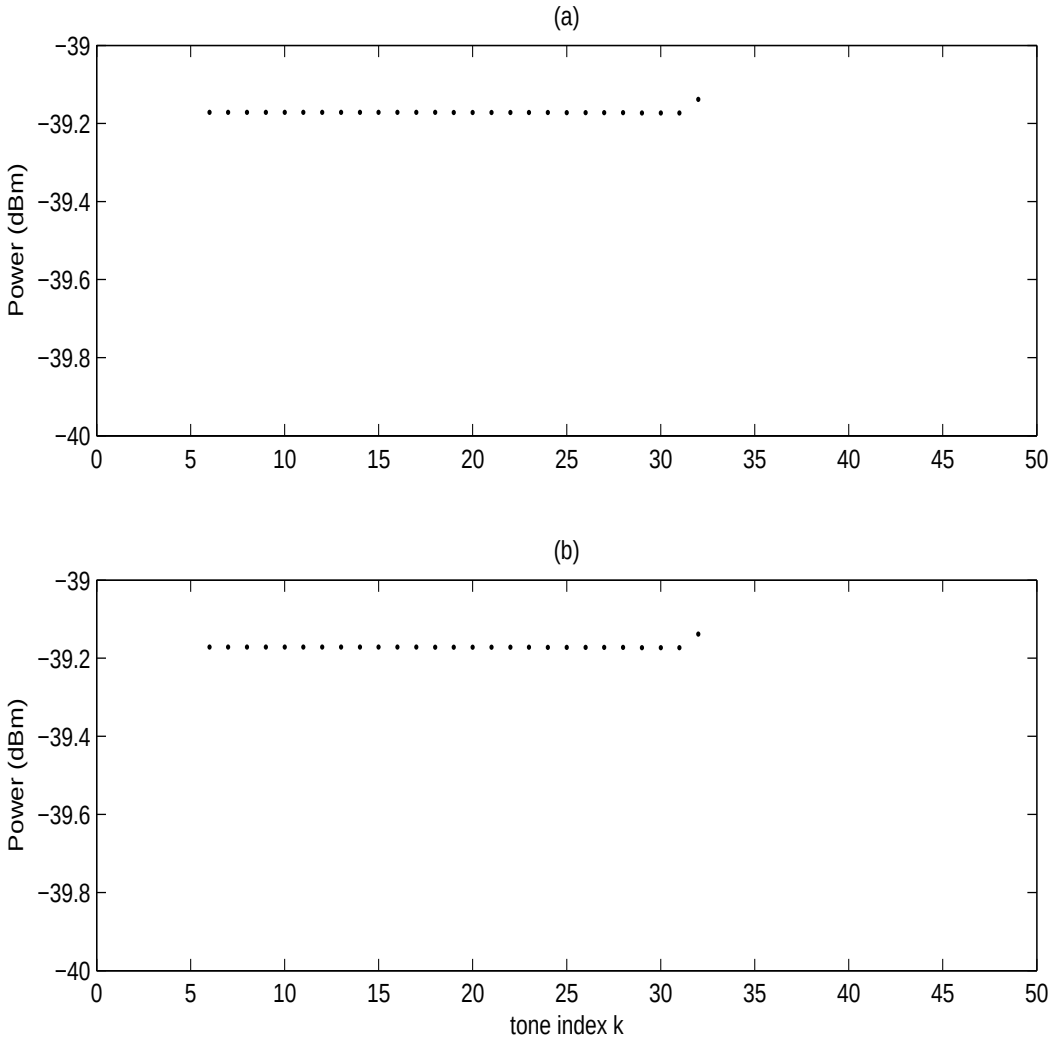

Figure 5.11: Power allocated to test loop 3 for upstream and Template M1 is used: (a) water-filling power allocation; (b) optimal power allocation.

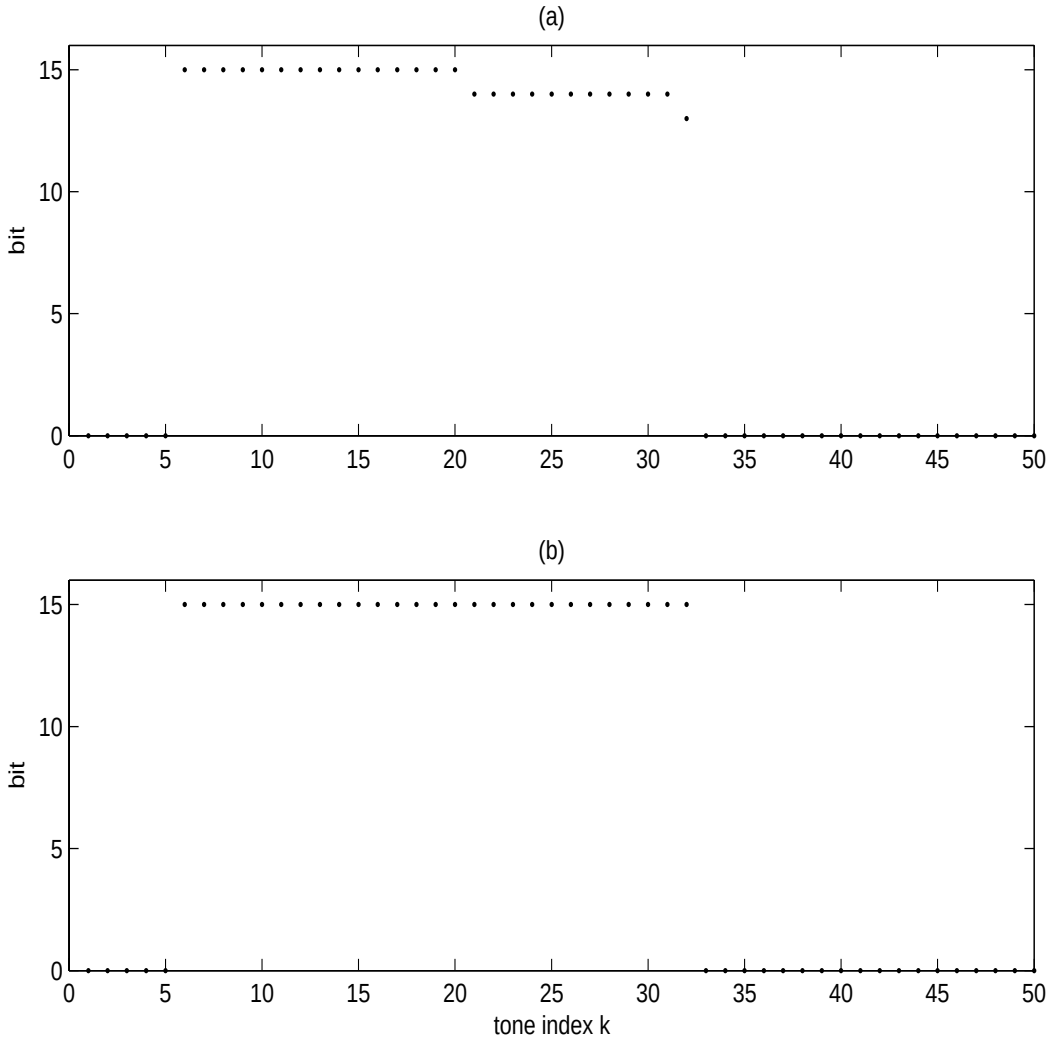

Figure 5.12: Bit allocated to test loop 2 for upstream and Template M1 is used: (a) water-filling power allocation; (b) optimal power allocation.

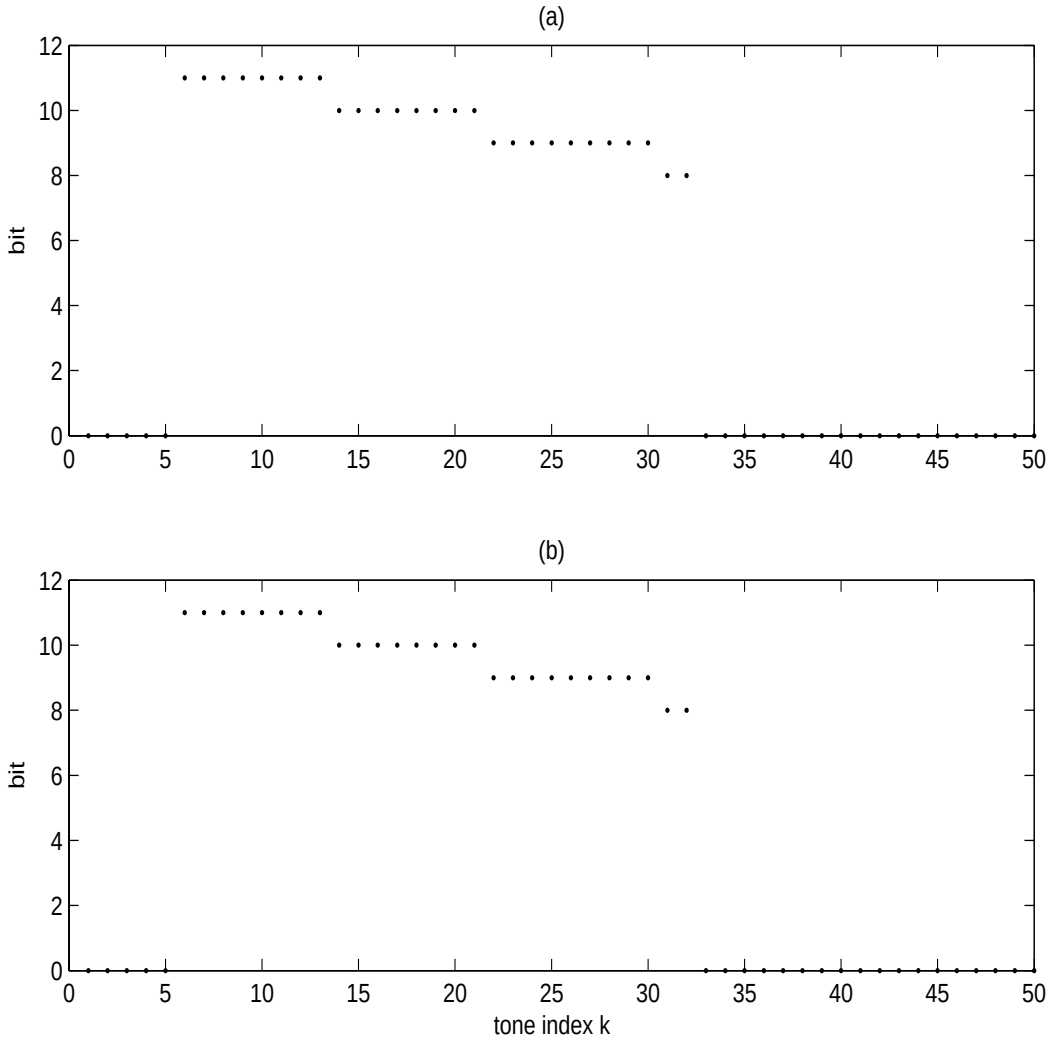

Figure 5.13: Bit allocated to test loop 3 for upstream and Template M1 is used: (a) water-filling power allocation; (b) optimal power allocation.

Table 5.1: Data rate of test loop for downstream. Template M1 is used. (Mbps)

loop	water-filling power allocation	optimal power allocation
test loop 1	71.392	71.968
test loop 2	22.944	23.936
test loop 3	6.592	6.880

Table 5.2: Data rate of test loop for upstream. Template M1 is used. (Mbps)

loop	water-filling power allocation	optimal power allocation
test loop 1	45.056	45.344
test loop 2	1.568	1.568
test loop 3	0.992	0.992

Table 5.3: Data rate of test loop for downstream. Template M2 is used. (Mbps)

loop	water-filling power allocation	optimal power allocation
test loop 1	76.512	76.512
test loop 2	26.048	26.336
test loop 3	7.040	7.168

Table 5.4: Data rate of test loop for upstream. Template M2 is used. (Mbps)

loop	water-filling power allocation	optimal power allocation
test loop 1	52.256	52.256
test loop 2	2.848	3.008
test loop 3	0.992	0.992

Table 5.5: Data rate of standard test loop for downstream. Template M1 is used. (Mbps)

loop	equal power allocation	optimal power allocation
VDSL1, long	57.184	59.200
VDSL2, long	58.336	60.160
VDSL3, long	56.928	58.656
VDSL4, long	39.680	41.824
VDSL5	77.408	77.408
VDSL6	35.776	37.440
VDSL7	22.176	23.456

Table 5.6: Data rate of standard test loop for upstream. Template M1 is used. (Mbps)

loop	equal power allocation	optimal power allocation
VDSL1, long	30.624	31.136
VDSL2, long	29.664	29.888
VDSL3, long	27.296	27.776
VDSL4, long	8.640	9.152
VDSL5	52.064	52.064
VDSL6	7.584	7.904
VDSL7	1.280	1.632

Table 5.7: Data rate of standard test loop for downstream. Template M2 is used. (Mbps)

loop	equal power allocation	optimal power allocation
VDSL1, long	62.144	62.176
VDSL2, long	63.168	63.232
VDSL3, long	61.728	61.760
VDSL4, long	44.224	44.448
VDSL5	81.984	81.984
VDSL6	40.000	40.320
VDSL7	25.184	25.184

Table 5.8: Data rate of standard test loop for upstream. Template M2 is used. (Mbps)

loop	equal power allocation	optimal power allocation
VDSL1, long	37.120	37.216
VDSL2, long	35.840	35.936
VDSL3, long	34.304	34.336
VDSL4, long	14.368	14.624
VDSL5	58.720	58.720
VDSL6	9.888	10.304
VDSL7	3.104	3.392

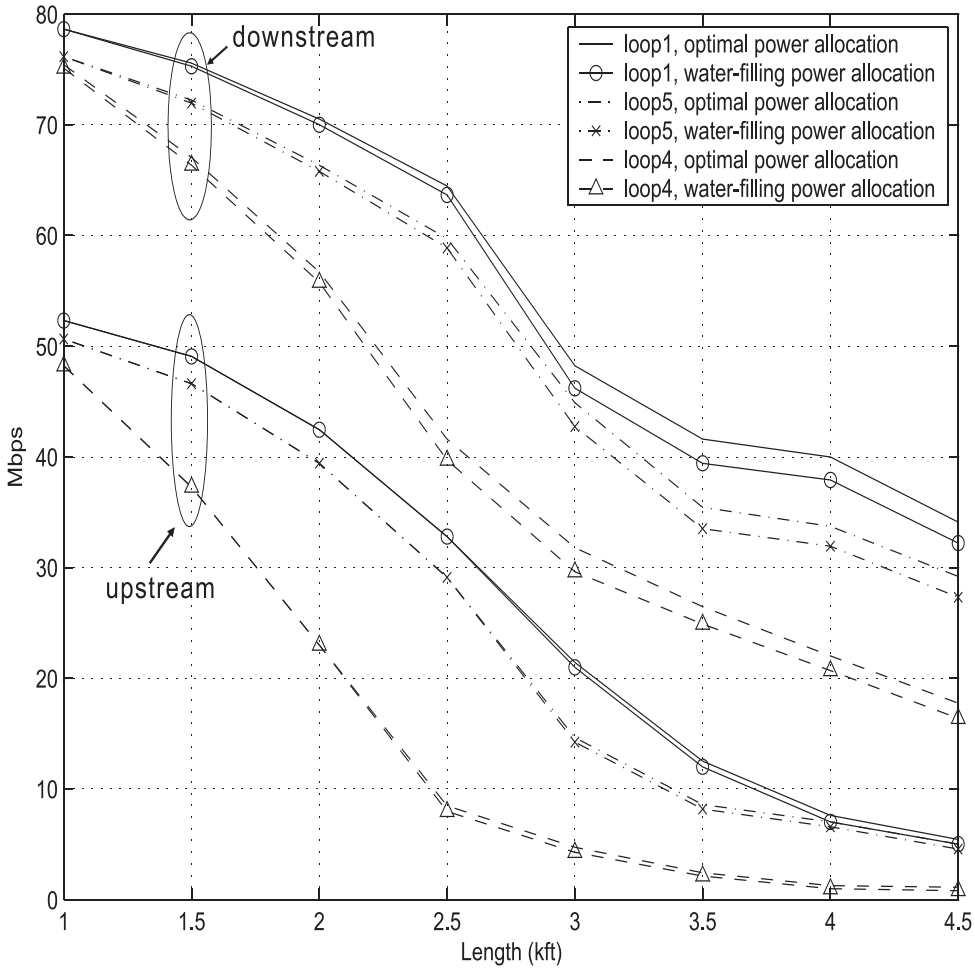

Figure 5.14: Data rate vs loop length for downstream and upstream. Template M1 is used.

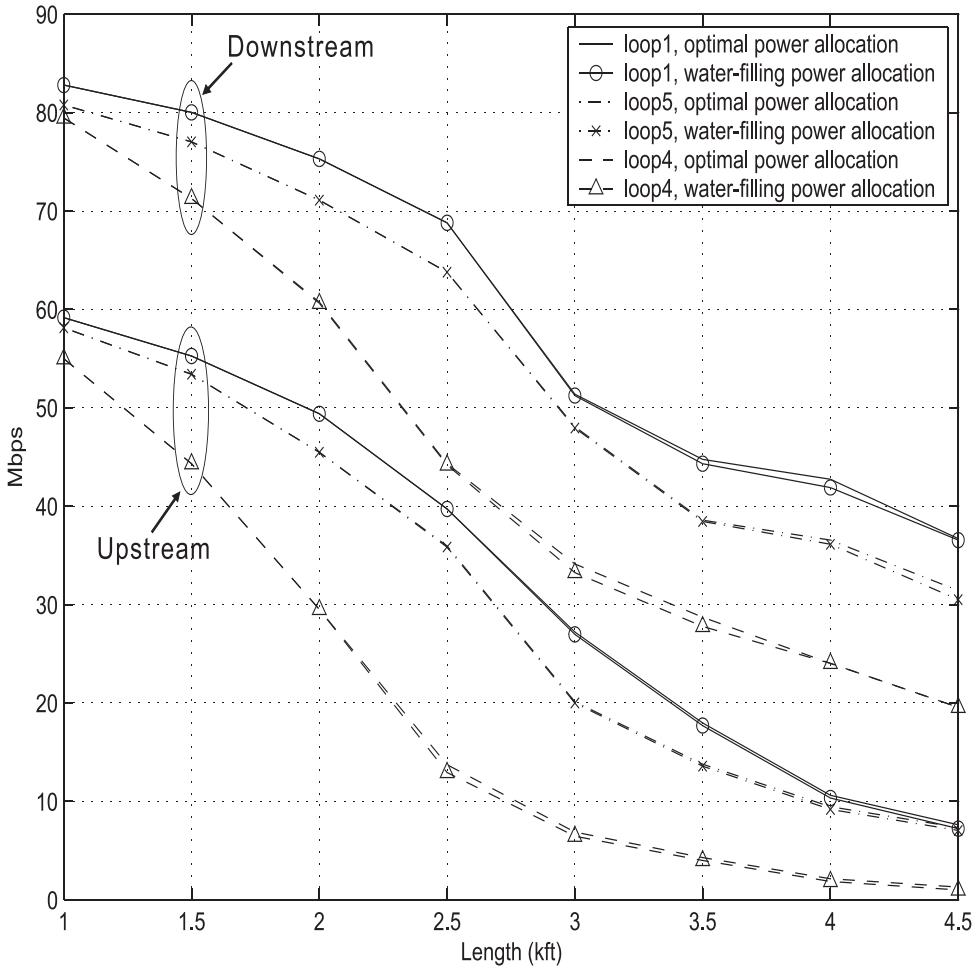

Figure 5.15: Data rate vs loop length for downstream and upstream. Template M2 is used.

Table 5.9: Results of grouping effect for downstream. Template M2 is used and g_{var} in dB. (Mbps)

group parameter (g_{number}, g_{var})	VDSL1 long	VDSL2 long	VDSL3 long	VDSL4 long
(256/0.5)	62.176/8	63.232/11	61.760/11	44.352/13
(256/1.0)	62.176/7	63.168/9	61.664/8	44.160/9
(256/2.0)	62.176/7	63.168/9	61.664/8	44.160/9
(512/0.5)	62.176/4	63.168/6	61.664/6	44.160/8
(512/1.0)	62.176/4	63.168/6	61.536/5	44.064/7
(512/2.0)	62.176/4	63.168/6	61.536/5	44.064/7

Table 5.10: Results of grouping effect for downstream. Template M2 is used and g_{var} in dB. (Mbps)

group parameter (g_{number}, g_{var})	VDSL5	VDSL5	VDSL7
(256/0.5)	81.984/6	40.320/13	25.216/6
(256/1.0)	81.984/6	40.192/9	25.216/6
(256/2.0)	81.984/6	40.192/9	25.216/6
(512/0.5)	81.984/3	40.192/8	25.216/4
(512/1.0)	81.984/3	40.128/7	25.216/4
(512/2.0)	81.984/3	40.128/7	25.216/4

Table 5.11: Results of grouping effect for upstream. Template M2 is used and g_{var} in dB. (Mbps)

group parameter (g_{number}, g_{var})	VDSL1 long	VDSL2 long	VDSL3 long	VDSL4 long
(256/0.5)	37.088/8	35.808/10	34.272/11	14.624/12
(256/1.0)	36.768/7	35.936/7	33.888/8	14.496/9
(256/2.0)	36.768/7	35.936/7	33.888/8	14.496/9
(512/0.5)	36.704/5	35.904/5	33.888/7	14.496/8
(512/1.0)	36.416/4	35.904/5	33.536/5	14.368/7
(512/2.0)	36.416/4	35.904/5	33.536/5	14.368/7

Table 5.12: Results of grouping effect for upstream. Template M2 is used and g_{var} in dB. (Mbps)

group parameter (g_{number}, g_{var})	VDSL5	VDSL5	VDSL7
(256/0.5)	58.720/5	10.304/7	3.392/6
(256/1.0)	58.720/5	10.304/7	3.392/6
(256/2.0)	58.720/5	10.304/7	3.392/6
(512/0.5)	58.720/3	10.304/4	3.392/4
(512/1.0)	58.720/3	10.304/4	3.392/4
(512/2.0)	58.720/3	10.304/4	3.392/4

Chapter 6

Conclusion

In this thesis, two power allocation methods are studied. For the conventional water-filling power allocation, we will clip the power allocated to subchannel if exceed the allowed maximum value and we do not have constraint on the non-zero power. Due to the clipping, we can not fully utilize the usable power to improve data rate. If the non-zero power allocated to a subchannel with large noise power, it might not be sufficient to transmit any bit and results in power wasted. Hence we introduce the optimal power allocation method, which take the channel condition into account. In this case, we examine the subchannel's SNR. If it is too low to allocate one bit, we turn off this subchannel and the usable power is allocated to the better subchannels. In this way we can improve the data rate by fully utilizing the usable power. From the experiments, we can see if the channel is not too short, we can get about 2 Mbps improvement on the data rate for downstream using Template M1. But for upstream the improvement is slight because the upstream bands are allocated on the high frequency band and they usually can not be used when the loop is long. Thus we can only improve the performance by allocating power to the optional band. However, this band is narrow and subject to the maximum bit constraint, the improvement is limited. We also propose one method to transmit the power allocation information to the transmitter. From the experiments, we can see that it might cause some loss on the data rate.

Bibliography

[1] P.P. Vaidyanathan, "*Multirate System and Filter Banks,*" Englewood Cliffs, Prentice-Hall, 1993.

[2] X. G. Gia, "*A New Precoding for ISI Cancellation Using Multirate Filterbanks,*" Proc. International Symposium on Circuits and Systems, Hong Knong,1997.

[3] S. D. Sandberg and M. A. Tzannes, "*Overlapped Discrete Multitone Modulation for Hign Speed Copper Wire Communications,*" IEEE J. Select. Areas Commun., Vol. 13, page(s):1571-1585, Dec. 1995.

[4] Yuan-Pei Lin and See-May Phoong, "*Perfect Discrete Multitone Modulation with Optimal Transceivers,*" Submitted to IEEE Tran. Signal Processing.

[5] T1.424/Trial-Use Standard, Very-high-bit-rate Digital Subscriber Line (VDSL) Metallic Interface, Part 1: Functional Requirement and Common Specification, "*Accredited Standards Committee T1,*" 2002.

[6] Thomas Starr, John M. Cioffi and Peter J. Silverman, "*Understanding Digital Subscriber Line Technology,*" Prentice-Hall, 1999.

[7] S.H. Tsai, "*Performance Evaluation of Optimal DMT Transceiver over ADSL,*" NCTU Taiwan, Master thesis, June 1999.

[8] C.C. Su, "*Transmitter and Receiver Windowing for OFDM Systems,*" NCTU Taiwan, Master thesis, July 2003.

[9] Igor Djokovic, "*MMSE Equalizers for DMT Systems with and without Crosstalk,*" Signals and Systems & Computers, 1997. Conference Record of the Thirty-First Asilomar Conference on Vol.1, Page(s): 545-549, 1998.

[10] Singiresu S. Rao, "*Engineering Optimization,*" Wiley Interscience, 1996.